


Calcofluor White-Phosphatidylethanolamine Conjugate-Enhanced Ethosomal Delivery of Voriconazole for Targeting *Candida albicans*

Ting Shen^{1,*}, Mengxing Li^{1,*}, Baocheng Tian^{1,*}, Wei Liu², Lili Chu³, Pengfei Yu¹, Huihui Zhou⁴, Yanchun Han¹, Chen Ding¹, Sixiang Sai¹

¹School of Pharmacy, Binzhou Medical University, Yantai, Shandong, 264003, People's Republic of China; ²College of Life and Health Science, Northeastern University, Shenyang, 110015, People's Republic of China; ³Department of Pathology, Yantai Fushan District People's Hospital, Yantai, Shandong, 265500, People's Republic of China; ⁴Department of Pathology, Affiliated Yuhuangding Hospital of Qingdao University, Yantai, Shandong, 266071, People's Republic of China

*These authors contributed equally to this work

Correspondence: Chen Ding, College of Life and Health Sciences, Northeastern University, Shenyang, 110015, People's Republic of China, Email dingchen@mail.neu.edu.cn; Sixiang Sai, School of Pharmacy, Binzhou Medical University, Yantai, Shandong, 264003, People's Republic of China, Email sixiang.sai@bzmc.edu.cn

Introduction: The increasing prevalence of systemic fungal infections, especially among immunocompromised individuals, highlights the need for advancements in targeted and effective antifungal treatments. This study presents a novel nanomaterial, CFW-phosphatidylethanolamine conjugate (CFW-PEc), designed to enhance the delivery and efficacy of antifungal agents by targeting fungal cell walls through specific chitin binding. Ethosomes, lipid-based nanocarriers known for their ability to improve drug delivery across skin and cell membranes, were utilized in this study.

Methods: The physicochemical characteristics of voriconazole-loaded CFW-PEc ethosomes (CFW-PEc-VRC-ethosomes) were examined, including particle size, zeta potential, and entrapment efficiency. Antifungal efficacy of CFW-PEc-VRC-ethosomes was evaluated, including antifungal activity in vitro, CFW-PEc-ethosomes cellular uptake, and models of animal infection and imaging analyses.

Results: In vitro experiments demonstrated a concentration-dependent inhibition of *C. albicans* growth by CFW-PEc, with cell inhibition rates reaching nearly 100% at 256 μ M. In vivo investigations confirmed a 5-fold reduction in fungal burden in the liver and a 7.8-fold reduction in the kidney compared to the control group following treatment with CFW-PEc (0.1 μ M)-VRC-ethosomes. Imaging analyses also confirmed the extended tissue retention of fluorescent dye-loaded CFW-PEc-ethosomes in mice, further underscoring their potential for clinical use.

Discussion: The targeted delivery of antifungal medications via ethosomes coated with CFW-PEc presents a promising strategy to improve antifungal effectiveness while reducing adverse effects, marking a significant advancement in fungal infection therapy.

Keywords: CFW-phosphatidylethanolamine conjugate, antifungal agents, fungal cell walls, chitin binding, ethosomes

Introduction

The incidence of fungal infections is increasingly threatening global public health. While many of these infections are superficial, certain fungal species have the potential to cause life-threatening illnesses. Individuals with compromised immune systems, such as organ transplant recipients, oncology patients, those with HIV/AIDS, and more recently, individuals with SARS-CoV-2, are at a heightened risk for fungal infections.¹⁻⁴ Systemic fungal infections typically originate in the lungs through inhalation of conidia (such as *Aspergillus* and *Cryptococcus*) or from endogenous microbiota (such as *Candida* species). Due to contaminated lines or leakage from the gastrointestinal tract and can spread to multiple organs in the host. Fatal infections caused by these pathogens result in over one million deaths globally

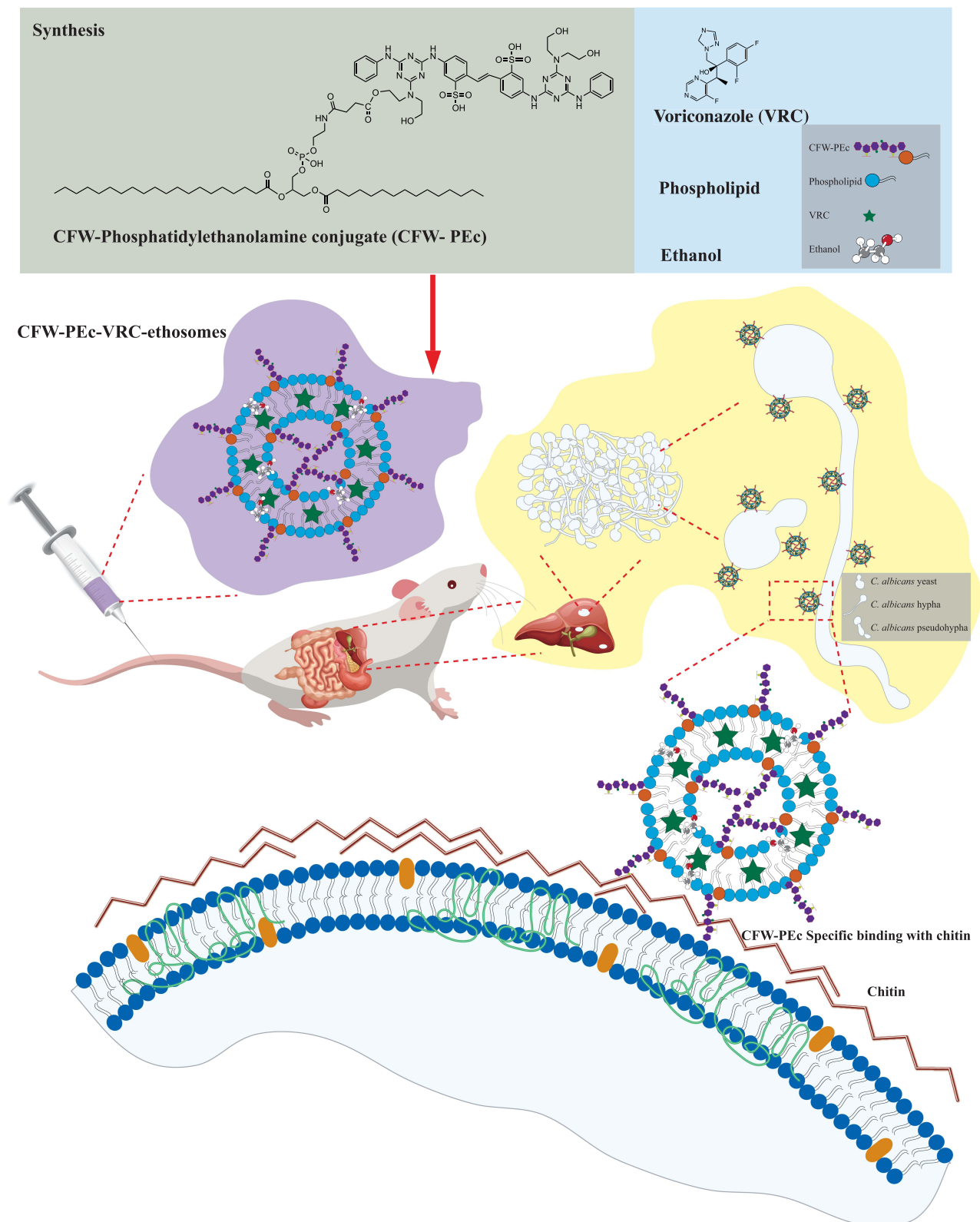
each year. Delayed initiation of appropriate therapy for systemic fungal infections can lead to medical emergencies with high mortality rates.^{5,6} *Candida albicans* is responsible for approximately 70% of *Candida* infections worldwide, posing a significant public health challenge with escalating severity.⁷ *C. albicans* can transition between yeast and filamentous forms, impacting its pathogenicity. Infections involve yeast cells attachment to host tissues and devices, forming biofilms resistant to host defenses and antifungal treatments, complicating clinical treatment.^{8,9}

The treatment of fungal infections usually entails the administration of four main classes of antifungals, namely polyenes, azoles, echinocandins, and pyrimidine analogues, which target different structures within fungal cells.¹⁰ Voriconazole is a broad-spectrum antifungal medication derived from fluconazole, belonging to the azole class, commonly used for treating and preventing invasive fungal infections.^{11–13} Therapeutic monitoring and prolonged maintenance dosages are necessary due to infection recurrence.^{14,15} The diversity in plasma levels among individuals undergoing voriconazole therapy presents a primary challenge, with this variability being impacted by factors including liver function, cytochrome P450 isoenzyme polymorphisms, drug interactions, as well as liver disease and cancer.^{16–19} Increased serum levels of voriconazole may lead to toxicity, presenting adverse effects such as phototoxicity, hallucinations, and hyponatremia.^{20,21}

Nanostructured systems present a promising strategy for enhancing antifungal therapy by reducing toxicity and improving drug targeting.^{22–25} The utilization of nanostructured systems in antifungal therapy dates back to the 1990s, particularly with the advancement of lipid formulations of amphotericin B.^{26,27} A significant aspect of nanotechnology in medicine lies in the advancement of drug delivery systems. Encapsulation of drugs in nanoparticles leads to a substantial increase in the therapeutic index compared to non-encapsulated drugs.²⁸ Nanostructures have the capacity to protect various compounds from enzymatic degradation, facilitate enhanced penetration through mucous epithelium, and regulate pharmacokinetics, thereby enhancing the efficacy of the active ingredient.^{29,30} Ethosomes are a lipid-based drug delivery system that uses high alcohol concentrations (20–45%) to enhance drug permeation, especially through skin. More flexible than traditional liposomes, ethosomes allow deeper penetration and better encapsulation of therapeutic agents. This targeted method makes ethosomes a promising approach for drug delivery, overcoming conventional system limitations.³¹

Fungal cell walls, including *C. albicans*, are structurally crucial for their function and interactions with the environment and immune recognition.^{32,33} They consist of fibrous and gel-like carbohydrate polymers forming a robust core scaffold, with proteins and superficial components added for strength and flexibility. The inner cell wall typically contains β -(1,3) glucan, chitin, and branched β -(1,6) glucan, with variations in composition among fungal species. In *C. albicans*, β -(1,6) glucan plays a key role in structural organization, linking β -(1,3) glucan and chitin.³⁴ This organization provides mechanical support close to the membrane and protection from degradative enzymes in the environment.^{35,36} Chitin is a unique component of fungal cell walls but absent in mammalian cells, making it an advantageous target. This specificity allows for the selective targeting of fungal cells without affecting host cells. By exploiting the inherent presence of chitin in fungal cell walls, drug delivery can be optimized through targeted interaction at the infection site, thereby enhancing therapeutic efficacy while minimizing side effects on surrounding healthy tissues. Calcofluor white (CFW), as a typical fluorescent brightener, is a valuable tool for detecting a range of yeasts and pathogenic fungi, including *C. albicans*, *Aspergillus* species, and *Cryptococcus neoformans*, due to its specific binding affinity with fungal components.^{37–39} CFW containing two sulfonic acid groups, enables solubilization under specific conditions, such as slight acidity, facilitating its interaction with β -linked glucans and nascent chitin chains.⁴⁰ This interaction disrupts chitin assembly by competitively binding to hydrogen bonding sites, thereby compromising fungal cell wall integrity and impeding fungal growth. Despite variations in cell wall structures between different fungi, CFW predominantly targets the chitin layer, causing perturbations across the entire cell wall structure.^{41,42} Notably, CFW is deemed safe for mammals, suggesting its potential utility in targeted delivery of antifungals.

In this study (Scheme 1), we synthesized CFW-phosphatidylethanolamine conjugate (CFW-PEc) as a nanomaterial with potent antifungal properties. The structure of CFW-PEc was elucidated using nuclear magnetic resonance spectroscopy. We also investigated the mechanism by which CFW-PEc interacts with its targets and determined its antifungal activity in fungi. Moreover, we developed fungal-targeted nano drug delivery systems based on CFW-PEc, including voriconazole-loaded CFW-PEc ethosomes (CFW-PEc-VRC-ethosomes), and studied their physicochemical



Scheme 1 Illustrative depiction of the therapeutic application of CFW-PEc-VRC-ethosomes in mice afflicted with fungal peritonitis. CFW-PEc, a synthesized compound derived from CFW and PE, is employed to formulate ethosomes encapsulating VRC. These ethosomes are administered intravenously to mice suffering from intraperitoneal infections caused by *C. albicans*. The structural characteristics of *C. albicans* promote the formation of biofilms at the infection sites, characterized by a loosely structured extracellular matrix predominantly composed of glucans, chitin, and various polymers. The interaction of CFW-PEc with chitin in the cell walls of *C. albicans* facilitates the targeted delivery of its ethosomes to the *Candida* infection sites via the bloodstream, thereby enhancing the therapeutic efficacy against the fungal pathogen.

characteristics such as particle size, zeta potential, and entrapment efficiency. The antifungal activity of these formulations against *C. albicans* yeast cells and hyphal cells was evaluated in vitro. Importantly, we characterized the drug delivery effectiveness of CFW-PEc-ethosomes in vitro and the distribution of CFW-PEc-Cy5.5-ethosomes in mice using small animal imaging. The antifungal activity of CFW-PEc-VRC-ethosomes was further examined in mice infection model. Meanwhile, the biosafety of CFW-PEc and CFW-PEc-VRC-ethosomes were determined, respectively, in vitro and in vivo. Our results provide compelling evidence that the innovative biomaterial CFW-PEc displays effective antifungal activity against *C. albicans* by exhibiting a specific binding affinity towards chitin located within the cell walls. The utilization of CFW-PEc has been shown to substantially improve the delivery efficiency and antifungal efficacy of nanoparticle-based treatments targeted against *C. albicans*. This enhancement provides a promising strategy for effectively reducing the fungal burden in mouse models of fungal peritonitis.

Methods

Materials and Strains

The materials used in this study included CFW, N-(3-dimethylaminopropyl)-N'-ethylcarbodiimide hydrochloride-crystalline (EDC·HCl), phosphatidylethanolamine (PE), N-hydroxysuccinimide (NHS), voriconazole (VRC), N-acetylglucosamine, polyoxin D, coumarin 6 (C6), cyanine 5.5 (Cy5.5), and phosphate buffered saline (PBS), all obtained from Sigma-Aldrich (St Louis, MO, USA). Crystal violet ammonium oxalate solution (1%, w/v) was obtained from Solarbio (Beijing, China). Purified water from Merck Millipore Ultrapure Water System (Darmstadt, Germany) was used in all experiments. All other chemicals and reagents were of analytical grade quality or higher.

The strains utilized were the sequenced reference strains *C. albicans* SC5314 and *C. neoformans* H99, purchased from the American Type Culture Collection (ATCC). The fungal cells were cultured on Yeast-peptone-dextrose (YPD) plates containing 1% (w/v) yeast extract, 2% (w/v) peptone, 2% (w/v) dextrose and 2% (w/v) agar; YPD broth including 1% (w/v) yeast extract, 2% (w/v) peptone, and 2% (w/v) dextrose; or spider medium including 1% (w/v) mannitol, 1% (w/v) yeast extract, and 0.2% (w/v) K₂HPO₄. A standard cell suspension was prepared by inoculating a single colony into YPD broth and incubating overnight at 30°C with shaking at 200 rpm. For in vitro antifungal activity and cellular uptake efficacy testing, *C. albicans* yeast cells were harvested, washed in PBS, and re-suspended in YPD broth at a concentration of 1×10^5 CFU/mL.

CFW-PEc Synthesis

PE and succinic anhydride were individually dissolved in anhydrous tetrahydrofuran by ultrasonication, and 1 mL of N, N-diisopropylethylamine (DIPEA) was drawn into a sterile syringe. DIPEA was added to the flask. After 2 days of reaction at 25°C in the dark condition, the reaction mixture was diluted with 4 times deionized water, and then dialyzed in deionized water using a dialysis bag for 4 days. The solution was centrifuged at 493 g for 5 minutes. The supernatant and precipitate were lyophilized by a freeze dryer and stored at 25°C. The supernatant was then further reacted with EDC·HCl, NHS, and CFW in a flask at 25°C in the dark condition. The reaction mixture was diluted with 4 times the volume of deionized water and then dialyzed in deionized water using a dialysis bag for 4 days. The solution was centrifuged at 493 g for 5 minutes. The final product was then lyophilized and stored at 25°C in the dark condition. The ¹H nuclear magnetic resonance (NMR) spectrum of PE in DMSO and CFW-PEc in DMSO was determined by NMR spectrometer (Bruker AM-400).

CFW-PEc Binding Assessment

To assess the binding capability of CFW-PEc, *C. albicans* and *C. neoformans* cultures were cultivated in YPD broth under various stress conditions. Initially, the cells were cultured overnight in YPD broth at 30°C with shaking at 200 rpm, then transferred to YPD broth supplemented with either 23 mM N-acetylglucosamine or 0.18 mM polyoxin D. After 6 hours of incubation at 30°C with shaking at 200 rpm., the cell cultures were diluted to a density of 1×10^7 CFU/mL. CFW-PEc was added to the YPD broth, and the cultures were incubated for 10 minutes at 30°C with shaking at 200 rpm. Additionally, the cells were cultured overnight in the YPD broth, and after 6 hours of incubation at 30°C with shaking at

200 rpm, they were diluted to a density of 1×10^7 CFU/mL. CFW-PEc, pre-incubated with chitin, was then added to the YPD broth, and the cultures were incubated for 10 minutes at 30°C with shaking at 200 rpm. Subsequently, the cells were washed twice with PBS and re-suspended in 200 μ L of PBS for fluorescence microscopy. Imaging was performed using a confocal laser scanning microscope (Leica TCS SPE) with a 63 \times oil immersion lens, exciting the cells with UV light below 365 nm, and capturing emission at 435 ± 10 nm.

The human breast cancer cell line MDA-MB-231 and the 293T cell line were obtained from the Type Culture Collection of the Chinese Academy of Sciences in Shanghai, China. 293T cells and MDA-MB-231 cells were cultured separately in DMEM at a concentration of 1×10^5 CFU/mL. Subsequently, 200 μ L of each cell culture was transferred to two laser confocal dishes and incubated for 3 hours at 37°C with 5% CO₂. Following this, the cultures were supplemented with 2 mL of DMEM and continued to incubate overnight at 37°C with 5% CO₂. The *C. albicans* SC5314 yeast cells, cultured overnight, were centrifuged at 493 g for 5 minutes, washed twice with PBS, resuspended in DMEM, and diluted to a concentration of 1×10^6 CFU/mL. Subsequently, 100 μ L of the diluted cell suspension was added to the confocal dishes containing the overnight-cultured 293T cells and MDA-MB-231 cells, respectively. Both 20 μ L of 0.2 mM CFW-PE and 20 μ L of Rhodamine B dye were added to each dish, and the cultures were incubated for 5 hours. Following the removal of the DMEM culture, the mixed cells were resuspended in 200 μ L of PBS. Imaging was conducted using the Leica TCS SPE equipped with a 63 \times oil immersion lens.

Preparation of CFW-PEc-VRC-Ethosomes and VRC-Ethosomes

CFW-PE-VRC-ethosomes and VRC-ethosomes were prepared using an ethanol injection method. Phospholipids (8 mg) and VRC (1 mg) were dissolved in 200 μ L of anhydrous ethanol under sonication. The resulting solution was injected into 800 μ L of deionized water under sonication to obtain 1 mL VRC-ethosomes. CFW-PEc (10 mg) was dissolved in 1 mL of DMSO, and phospholipids (8 mg) were dissolved in 199 μ L of anhydrous ethanol. The CFW-PEc solution was mixed with the prepared solution and injected into water under sonication to obtain 1 mL of CFW-PEc (1 μ M)-VRC-ethosomes. Similarly, CFW-PEc (0.1 μ M)-VRC-ethosomes and CFW-PEc (0.01 μ M)-VRC-ethosomes were prepared following the same procedure.

Characterization of CFW-PEc -VRC-Ethosomes and VRC- Ethosomes

The protocol was performed as described elsewhere.⁴³ Basically, the particle size and zeta potential of nanoparticles were analyzed using dynamic light scattering with a Zetasizer Nano-ZS ZEN3600 (Malvern Instruments Ltd, Worcestershire, UK) at 25°C after diluting the nanoparticles in deionized water. The entrapment efficiency (EE) and drug loading capacity (DL) of VRC were determined through indirect calculations: 1 mL of nanoparticles was centrifuged at 1972 g using an ultrafiltration tube (Millipore, USA, MWCO 10 kDa) for 10 minutes to separate the free drug (W_{free}) and encapsulated VRC (W). The filtrate collected was analyzed for free VRC content using high-performance liquid chromatography with a C¹⁸ reversed-phase column (5 μ m) and a mobile phase ratio of methanol to 0.1% acetic acid of 70:30 at a flow rate of 1.0 mL/min, detection at 256 nm, column temperature set at 30°C, and an injection volume of 20 μ L. Total VRC (W_{total}) in nanoparticles was determined by disrupting the nanoparticles with a mixture of 900 μ L methanol and 100 μ L of nanoparticles. W_{lip} represents the total amount of lipid materials used for ethosomes preparation. EE (%) and DL (%) were then calculated using the following formulas. The stability of the nanoparticles during storage was evaluated by monitoring changes in particle size and zeta potential at 25°C over a period of 2 weeks.

$$EE\% = \frac{W_{\text{total}} - W_{\text{free}}}{W_{\text{total}}} \times 100 \quad (1)$$

$$DL\% = \frac{W_{\text{total}} - W_{\text{free}}}{W_{\text{total}} - W_{\text{free}} + W_{\text{lip}}} \times 100 \quad (2)$$

In vitro Antifungal Efficacy

The antifungal efficacy of the compounds against *C. albicans* yeast cells was assessed in the YPD broth according to protocols from the National Committee for Clinical Laboratory Standards (M27-A3). Serial dilutions of CFW-PEc, ranging from 8 μM to 512 μM , and serial dilutions of CFW-PEc (0.01–1 μM)-VRC-ethosomes and VRC-ethosomes (0.015 to 32 $\mu\text{g}/\text{mL}$) were prepared in YPD broth. These dilutions were added to the first 10 rows of a 96-well plate (100 μL per well) using a multichannel pipette. Each well received 100 μL of YPD broth containing 1×10^5 CFU/mL of *C. albicans* yeast cells. Control wells contained 1×10^5 CFU/mL in 100 μL of YPD broth and 100 μL of drug-free YPD broth. The plates were incubated at 30°C with shaking at 200 rpm for 12 hours, and optical density at 600 nm was measured using a microplate spectrophotometer to determine the percentage inhibition of *C. albicans* growth relative to the control. Each assay was conducted in duplicate and repeated three times.

The antifungal efficacy of the compounds against *C. albicans* biofilm formation was evaluated using the crystal violet method. A single colony of *C. albicans* SC5314 was selected and inoculated into 5 mL of YPD broth, then incubated overnight at 30°C with shaking at 200 rpm. The resulting culture was centrifuged at 493 g for 5 minutes, washed twice with PBS, resuspended in a spider medium containing 10% fetal bovine serum, and the OD value was measured at 600 nm using a UV spectrophotometer. The density of *C. albicans* SC5314 was diluted to 1×10^4 CFU/mL, and 100 μL of the diluted culture along with 100 μL of the compound-containing samples (final concentrations of 4 $\mu\text{g}/\text{mL}$ and 8 $\mu\text{g}/\text{mL}$) in spider medium with 10% fetal bovine serum were added to each well of a 96-well plate. Control groups consisted of 100 μL of the diluted culture with 100 μL of spider medium, while blank controls received 200 μL spider medium. The plate was then incubated for 24 hours at 37°C with shaking at 200 rpm. Following three washes with sterile PBS, 0.1% crystal violet solution was added and allowed to stain for 15 minutes. Excess stain was removed with sterile water, followed by elution with 95% ethanol for 15 minutes. The eluate was transferred to a new 96-well plate, and the OD value was measured at 595 nm.

Cytotoxicity Assay of CFW-PEc and CFW-PEc (0.01 μM –1 μM)-VRC-Ethosomes

CFW-PEc-ethosomes were prepared with CFW-PEc at concentrations from 0.01 μM to 1 μM through ethanol injection. Similarly, CFW-PEc-VRC-ethosomes were loaded with VRC at 50 $\mu\text{g}/\text{mL}$. After filtration through a 0.22 μm membrane, the preparations were diluted 10 times with DMEM medium. 293T cells in DMEM medium were washed twice with 2 mL of PBS. 1 mL of EDTA-trypsin was then added and incubated for 30 seconds. Following this, 2 mL of DMEM medium was added to terminate the digestion. 293T cells were centrifuged at 190 g for 5 minutes and adjusted to a density of 5×10^4 CFU/mL during the logarithmic phase. Each well of a 96-well plate received 180 μL of the cell suspension and was incubated overnight at 37°C with 5% CO_2 . The sample groups were treated with 20 μL of the prepared CFW-PEc-ethosomes and CFW-PE-VRC-ethosomes, while the control groups received 20 μL of drug-free DMEM medium. The plate was then incubated at 37°C with 5% CO_2 for 12 hours. For the cytotoxicity assay of CFW-PEc, 293T cells were prepared as described earlier and exposed to varying concentrations of CFW-PEc (0.01–1 μM) in each well, incubated at 37°C with 5% CO_2 for 12 hours. Cytotoxicity was assessed using the Cell Counting Kit-8 (Sigma-Aldrich, St Louis, MO, USA) reduction assay, and the OD value was measured at 450 nm. Cell viability percentages were calculated relative to the control using GraphPad Prism v.9.0. All experiments were conducted in duplicate and repeated three times.

CFW-PEc-Ethosomes Cellular Uptake

The cellular uptake of CFW-PEc-ethosomes by *C. albicans* cells was evaluated using coumarin-based fluorescent ethosomes. CFW-PE (0.01–1 μM)-C6-ethosomes and C6-ethosomes were prepared and diluted to a concentration of 0.2 $\mu\text{g}/\text{mL}$. For the investigation of nanoparticle uptake in *C. albicans* yeast cells, 20 μL of C6 dye solutions were added to each well of a 24-well plate containing 1.98 mL of YPD medium with 1×10^5 CFU/mL *C. albicans* yeast cells. The plates were shielded from light and incubated at 30°C. In the study of nanoparticle uptake in *C. albicans* hyphal cells, *C. albicans* yeast cells in YPD medium were washed twice with PBS, resuspended in spider medium containing 5% fetal bovine serum. 20 μL of C6 dye solutions were added to each well of a 24-well plate containing 1.98 mL of spider

medium with 4×10^5 CFU/mL *C. albicans* yeast cells. The plates were shielded from light and incubated at 37°C. At 3, 6, and 9 hours post-treatment, 400 μ L of fungal cells were collected, washed, and resuspended in 100 μ L of PBS for imaging using a Leica TCS SPE. Fluorescence was captured with two distinct UV light excitation wavelengths, with emissions collected at 490 ± 10 nm for C6 and 435 ± 10 nm for CFW-PEc. The assays were conducted in duplicate and repeated five times.

In vivo Animal Imaging Analysis

Kunming mice aged 4–5 weeks and weighing 14–16 g were procured from Jinan Pengyue Experimental Animal Breeding Co., LTD (Jinan, Shandong, China) for the in vivo imaging study. Twenty mice were randomly chosen and divided evenly ($n = 4$) into five groups. A single colony of *Candida albicans* SC5314 was inoculated into 5 mL of YPD broth, followed by overnight incubation at 30°C with shaking at 200 rpm. The cell cultures were centrifuged at 493 g for 5 minutes and washed twice with PBS. The cell suspension was adjusted to a concentration of 2×10^8 CFU/mL. Each mouse received an intraperitoneal injection of 200 μ L of the cell suspension. In the control group, 200 μ L of PBS was injected intraperitoneally. CFW-PEc (0.01–1 μ M)-Cy5.5-ethosomes and Cy5.5-ethosomes were prepared for the study. After 7 days post-infection, infected mice were administered 200 μ L of Cy5.5-loaded nanoparticles via the tail vein. Additionally, uninfected mice received an injection of CFW-PEc (0.1 μ M)-Cy5.5-ethosomes. Fluorescence imaging was conducted using an IVIS Spectrum In Vivo Imaging System (PerkinElmer, USA) at five time points post-treatment: 1.5 hours, 4 hours, 6 hours, 8 hours, and 24 hours for data collection and analysis.

In vivo Antifungal Efficacy

For the CFU assay, CFW-PEc (0.01–1 μ M)-VRC-ethosomes, VRC-ethosomes, and VRC in solution were prepared and dissolved in sterile saline. Sixty mice were randomly selected and divided equally into six groups. Intraperitoneal infection was described in the in vivo animal imaging analysis. One day after infection, the mice were intravenously administered 2 mg/kg of the test drugs. Control group mice received PBS at the same dosage. After 8 days post-infection, seven mice from each group were sacrificed, and their liver and kidney tissues were isolated, weighed, and placed in 10 mL of PBS. The tissues were homogenized, and the resulting suspension was plated on YPD agar and incubated at 30°C for 2 days to determine the colony-forming units. Additionally, for histopathological assessment, three mice from each group were sacrificed at 8 days post-infection, and their liver and kidney tissues were collected and stained with Hematoxylin and Eosin (H&E).

Image Analysis

Image analysis was performed using ImageJ, a software developed by the National Institutes of Health, for image compilation and analysis. In the study of the cellular uptake efficiency of CFW-PEc-ethosomes in vitro, the mean gray value of nanoparticle fluorescence intensity was determined by dividing the total intensity across cells by the cell area. Statistical significance was assessed by measuring five images per experimental group. For the in vivo animal imaging analysis, the total flux of nanoparticle fluorescence intensity in the peritoneal cavity of mice was quantified using Living Image software (version 4.4). Individual measurements were taken for each mouse in every experimental group to ensure accurate data collection.

Statistical Analysis

Experiments were repeated independently at least three times for reproducibility, with data presented as the mean \pm SD. Statistical significance was determined using ANOVA and Tukey's test (SPSS 19.0; IBM, Armonk, NY, USA), with a significance threshold set at $P \leq 0.05$.

Results and Discussion

Characterization of CFW-PEc Structure

The synthesis scheme of CFW-PEc is shown in [Figure 1A](#). The first step involves the reaction of succinic anhydride with the amino group in PE under alkaline conditions to generate a carboxyl group, producing the intermediate product PE-succinic anhydride. The second step involves the esterification reaction between the intermediate product and CFW to produce CFW-PEc. The structure of the final product was determined through NMR spectroscopy analysis. The ^1H NMR spectrum of PE in DMSO and the synthesized product in DMSO are presented in [Figure 1B](#) and [C](#), respectively. Remarkably, [Figure 1C](#) displays two additional sets of peaks compared to [Figure 1B](#). The signals observed at δ 3.6–3.7 ppm were assigned to the CH_2 protons of CFW, while the peaks at δ 6.0–8.0 ppm indicated the presence of an anomeric hydrogen of CFW. These results indicate a complete linkage between CFW and PE-succinic anhydride, confirming the successful synthesis of CFW-PEc. The synthesis of novel CFW-PEc through a coupling of CFW with PE via the succinic anhydride reaction is a significant innovation. This unique synthetic method allows for precise functionalization designed for specifically targeting fungal cells, distinguishing our approach from previously developed antifungal nanoparticle systems.⁴⁴

CFW-PEc Exhibits Specific Binding to Chitin Within the Cell Walls

CFW is a diaminostilbene derivative that emits fluorescence under UV light and has a selective affinity for β -linked fibrillar polymers such as cellulose and chitin, forming attachments through hydrogen bonding.³⁹ In order to determine if CFW-PEc could replicate the interaction between CFW and chitin in fungal cell walls, a specific binding test was performed between CFW-PEc and its substrate. In *C. albicans* yeast cells cultured in YPD broth and treated with CFW-PEc, a typical CFW fluorescence pattern was observed in the cell wall ([Figure 2A](#)). The fluorescence intensity of CFW-PEc in yeast cells cultured in YPD broth supplemented with 23 mM N-acetylglucosamine exhibited a significant increase compared to the control cells ([Figure 2B](#)). In contrast, yeast cells cultured in YPD broth with 0.18 mM polyoxin D displayed a marked decrease in fluorescence intensity ([Figure 2C](#)). Furthermore, the fluorescence intensity of CFW-PEc in yeast cells treated with CFW-PEc that had been preincubated with chitin was nearly undetectable ([Figure 2D](#)). In *C. neoformans* cells, similar patterns of CFW-PEc fluorescence were observed ([Figure 2E–H](#)). The growth of fungi cells on N-acetylglucosamine-enriched medium stimulates chitin synthesis, resulting in elevated chitin levels in the cell wall.⁴⁵ In contrast, polyoxin D impacts septum formation, cell wall maturation, and bud ring formation, leading to impaired fungal cell growth due to its inhibition of chitin polymerization.⁴⁶ Our findings suggest a strong correlation between the fluorescence intensity of CFW-PEc in *C. albicans* and *C. neoformans* cells and alterations in chitin synthesis. The fluorescence intensity of CFW-PEc in fungi cells serves as a reliable indicator of the chitin levels in the cell wall. Hence, it is reasonable to infer that CFW-PEc retains the capacity to bind to chitin chains in the cell wall inherited from CFW.

To investigate the selective binding of CFW-PEc to chitin in the fungal cell wall compared to mammalian cells, a binding assay was performed using *C. albicans* yeast cells and mammalian cells. As depicted in [Figure 2I](#), the fluorescence intensity of CFW-PEc was exclusively detected in *C. albicans* yeast cells rather than in 293T cells. Similarly, a consistent pattern of fluorescence intensity of CFW-PEc was observed in the co-culture of MDA-MB-231 cells and *C. albicans* yeast cells ([Figure 2J](#)). These findings suggest that CFW-PEc demonstrates a preference for binding to fungal cells over mammalian cells through specific interactions with chitin in the fungal cell wall. The ability of CFW-PEc to selectively bind to chitin in fungal cell walls marks a significant advancement in antifungal therapy. While there are other antifungal nanoparticles available, many of them lack specificity toward fungal structures, which can result in off-target effects and reduced safety, thereby limiting their application in the clinical field.^{47,48} CFW-PEc's clear preference for fungal cells, without interacting with mammalian cells, may minimize potential cytotoxicity and enhance the therapeutic index, making it a promising candidate for safer antifungal treatments.

In vitro Assessment of the Antifungal Activity and Cytotoxicity of CFW-PEc

To investigate the antifungal activity of CFW-PEc against *C. albicans* yeast cells, an in vitro antifungal activity assay was conducted in YPD broth. The results presented in [Figure 2K](#) demonstrate a concentration-dependent inhibition rate of

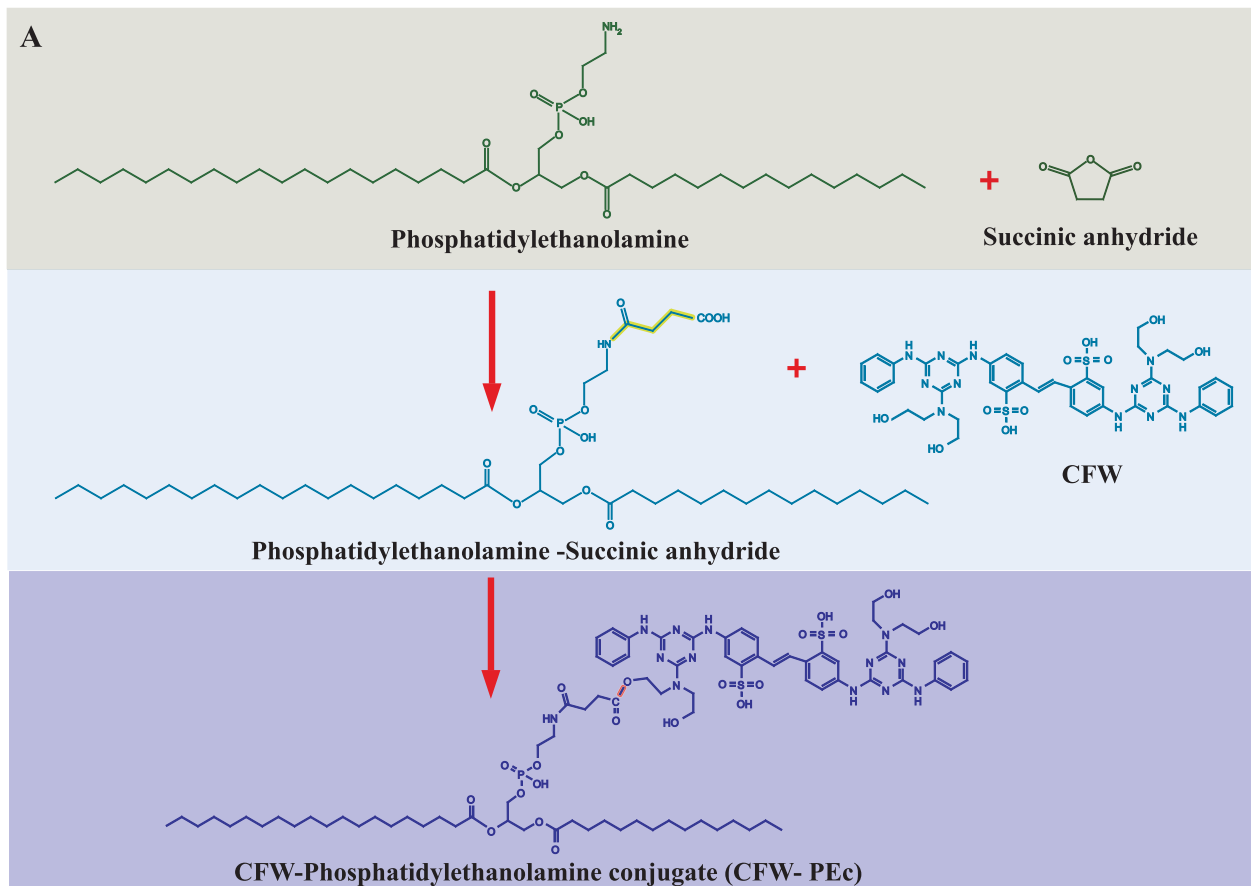
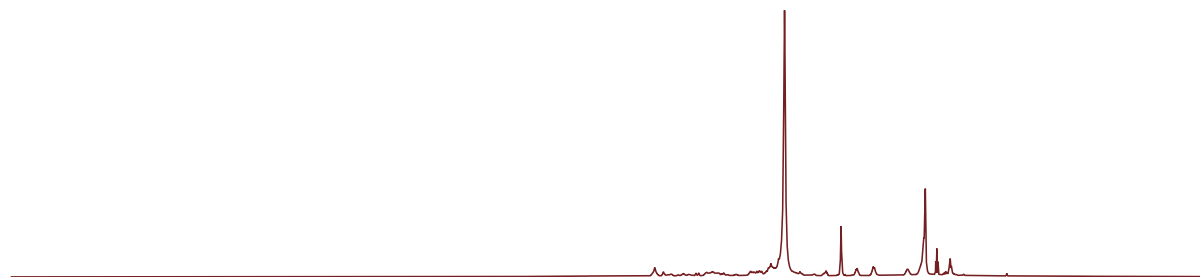
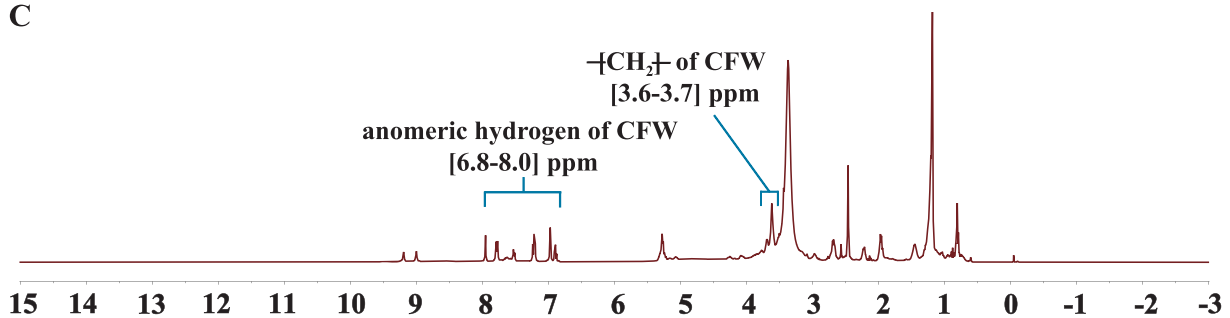
**B****C**

Figure 1 (A) Schematic diagram illustrating the two-step synthesis of CFW-PEc, where succinic anhydride reacts with PE to form an intermediate followed by esterification with CFW to yield CFW-PEc. (B) ^1H NMR spectrum of PE in DMSO, demonstrating the initial reactant's characteristics. (C) ^1H NMR spectrum of the synthesized CFW-PEc, highlighting the additional peaks that confirm the successful formation of CFW-PEc.

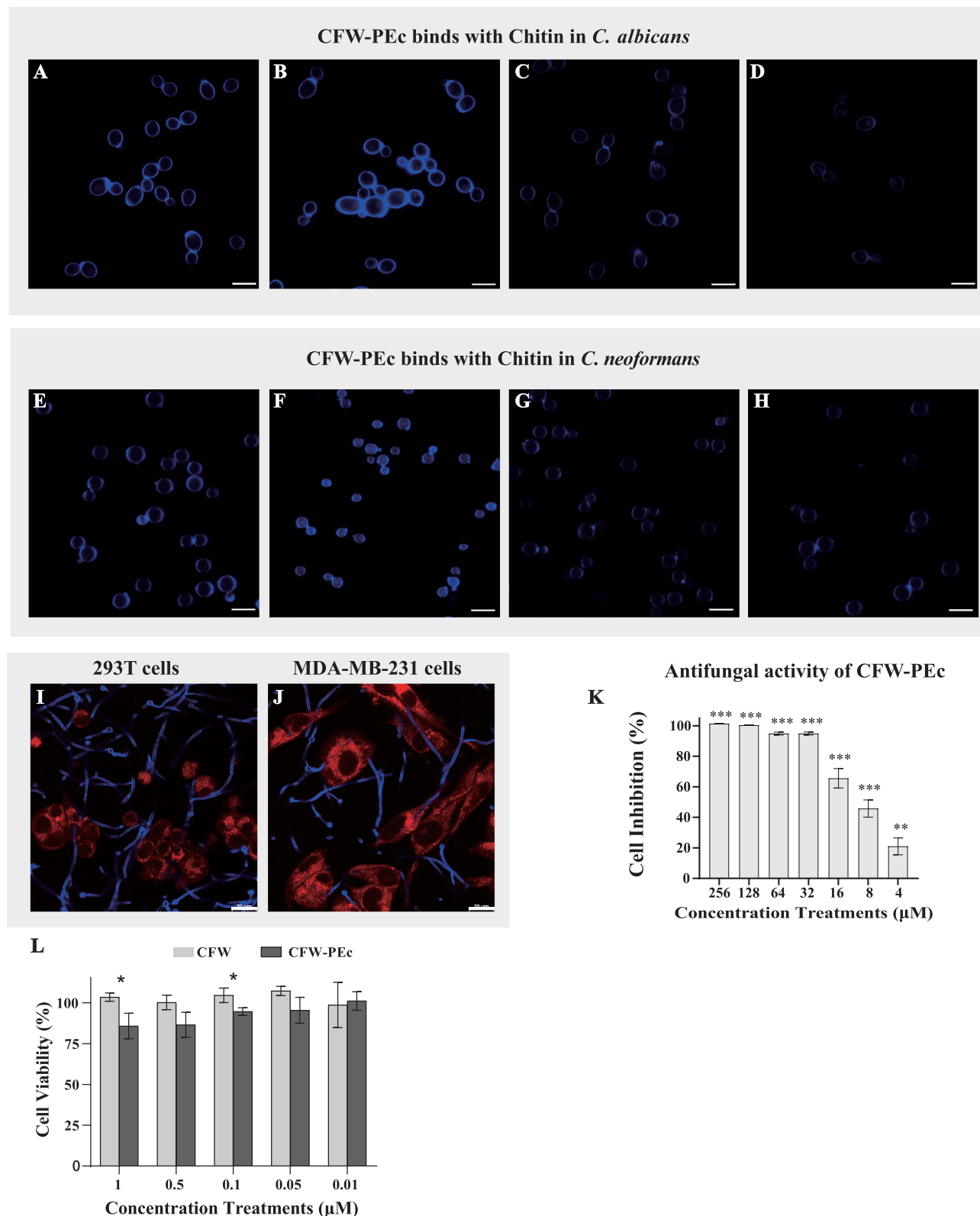


Figure 2 (A) Fluorescence imaging showing specific localization of CFW-PEc in the cell wall of *C. albicans* yeast cells cultured in YPD broth. (B) Significant enhancement in fluorescence intensity of CFW-PEc in yeast cells supplemented with 23 mM N-acetylglucosamine, indicating increased binding to chitin. (C) Noticeable reduction in fluorescence intensity with 0.18 mM polyoxin D treatment, suggesting impairment in chitin binding. (D) Minimal fluorescence detected in yeast cells treated with CFW-PEc preincubated with chitin, indicating competitive inhibition of binding. (E–H) Fluorescence imaging patterns in *C. neoformans* cells, similar to those observed in *C. albicans*. Scale bars are 10 μm. (I) CFW-PEc fluorescence was exclusively detected in *C. albicans* yeast cells, indicating specificity for fungal cells over 293T cells. (J) CFW-PEc fluorescence in co-culture with MDA-MB-231 cells demonstrates selective retention in *C. albicans*. Scale bars are 20 μm. (K) Inhibition rates of CFW-PEc against *C. albicans* yeast cells, highlighting significant efficacy across concentrations (**P ≤ 0.01; ***P ≤ 0.001). (L) Viability comparison of 293T cells treated with CFW versus CFW-PEc, indicating relative safety with CFW-PEc treatment (*P ≤ 0.05).

CFW-PEc, with the maximum cell inhibition rate reaching nearly 100% at a concentration of 256 μM . Conversely, the minimum cell inhibition rate of CFW-PEc against *C. albicans* yeast cells was approximately 21% at a concentration of 4 μM . In fungi, the antifungal activity of CFW is attributed to its binding to chitin chains. Therefore, the preservation of antifungal efficacy in CFW-PEc, following its formation from CFW, is not surprising. Additionally, an in vitro cytotoxicity assay was performed to assess the safety profile of CFW-PEc in mammalian cells. The cell viability of 293T cells treated with CFW-PEc was compared to that of cells treated with a PBS solution, as shown in Figure 2L. The cell viability of 293T cells exposed to CFW-PEc at a concentration of 1 μM was approximately 86%, which increased to around 95% at a concentration of 0.1 μM . These findings suggest that CFW-PEc exhibits a favorable safety profile in vitro.

Characterization of CFW-PEc-VRC-Ethosomes and VRC-Ethosomes

Nanoparticles offer the potential to mitigate unfavorable drug characteristics and enhance drug permeation across biological membrane barriers, thereby facilitating the treatment of deep-seated fungal infections.⁴⁴ Essential nanoparticle properties, including particle size and zeta potential, play a crucial role in their ability to adhere to and interact with biological cells, facilitate drug release, promote brain penetration, and enhance cellular uptake efficiency.⁴⁹ The particle size and zeta potential of nanoparticles were characterized using dynamic light scattering. The particle size distributions of CFW-PEc (0.01–1 μM)-VRC-ethosomes and VRC-ethosomes are depicted in Figure 3A–H, with detailed distributions shown in Figure 3A and B for VRC-ethosomes, and Figure 3C–H for CFW-PEc (0.01 μM), (0.1 μM), and (1 μM)-VRC-ethosomes, respectively, while the average of particle size and zeta potential is listed in Table 1. Notably, the polydispersity index (PDI) of CFW-PEc (0.1 μM and 1 μM)-VRC-ethosomes was lower than that of VRC-ethosomes, indicating a more centralized particle size distribution. Furthermore, the particle sizes of CFW-PEc (0.01–1 μM)-VRC-ethosomes and VRC-ethosomes were measured at 94.32 ± 0.045 nm, 95.08 ± 0.28 nm, 95.93 ± 0.63 nm, and 98.63 ± 1.19 nm, respectively. These findings indicate that inclusion of CFW-PEc does not significantly alter particle sizes. The zeta potential values for CFW-PEc (0.01–1 μM)-VRC-ethosomes and VRC-ethosomes were determined to be -33.1 ± 0.7 mV, -28.9 ± 0.6 mV, -23.25 ± 1.05 mV, and -21.9 ± 0.4 mV, respectively. Of particular note is the slight decrease in negative zeta potential of CFW-PEc-VRC-ethosomes, which contributes to the steric stabilization of nanoparticles at the particle/water interface.⁵⁰ Efficient drug entrapment efficiency (EE) and drug loading (DL) are crucial parameters for evaluating drug delivery systems.⁵¹ As illustrated in Table 1, the EE (%) of VRC-ethosomes was recorded at $53.35 \pm 0.51\%$, with a DL (%) of $6.51 \pm 0.06\%$; while the EE of CFW-PEc (0.01–1 μM)-VRC-ethosomes ranged from $39.20 \pm 0.96\%$ to $43.67 \pm 2.15\%$, with a DL of $4.78 \pm 0.12\%$ to $5.33 \pm 0.26\%$. Figure 3I and J show that there were no notable alterations in the particle size and zeta potential of CFW-PEc (0.01–1 μM)-VRC-ethosomes following a 2-week storage period at 25°C, suggesting exceptional storage stability.

In vitro Antifungal Activity of CFW-PEc-VRC-Ethosomes and Cytotoxicity of CFW-PEc-VRC-Ethosomes

The antifungal activity of CFW-PEc-VRC-ethosomes was evaluated through an in vitro antifungal activity test conducted in YPD broth containing *C. albicans* yeast cells. The test compared the effects of CFW-PEc (0.01–1 μM)-VRC-ethosomes, VRC-ethosomes, and VRC, with the results summarized in Figure 4A. The inhibition rates of the five components demonstrated significant efficacy against *C. albicans* yeast cells, with cell inhibition rates exceeding 60%. No substantial differences in cell inhibition rates were observed between VRC-ethosomes and VRC across all concentrations. While the inhibition rates of CFW-PEc (0.01 μM and 0.1 μM)-VRC-ethosomes were slightly lower than those of VRC, the differences were generally, generally, around 3% in most cases. Interestingly, CFW-PEc (1 μM)-VRC-ethosomes exhibited markedly reduced growth inhibition effects at all concentrations compared to the other four components. These results suggest that CFW-PEc-VRC-ethosomes could preserve the antifungal activity of VRC in vitro. Importantly, the presence of a high concentration of CFW-PEc (1 μM) was found to compromise the drug delivery efficiency of VRC in vitro.

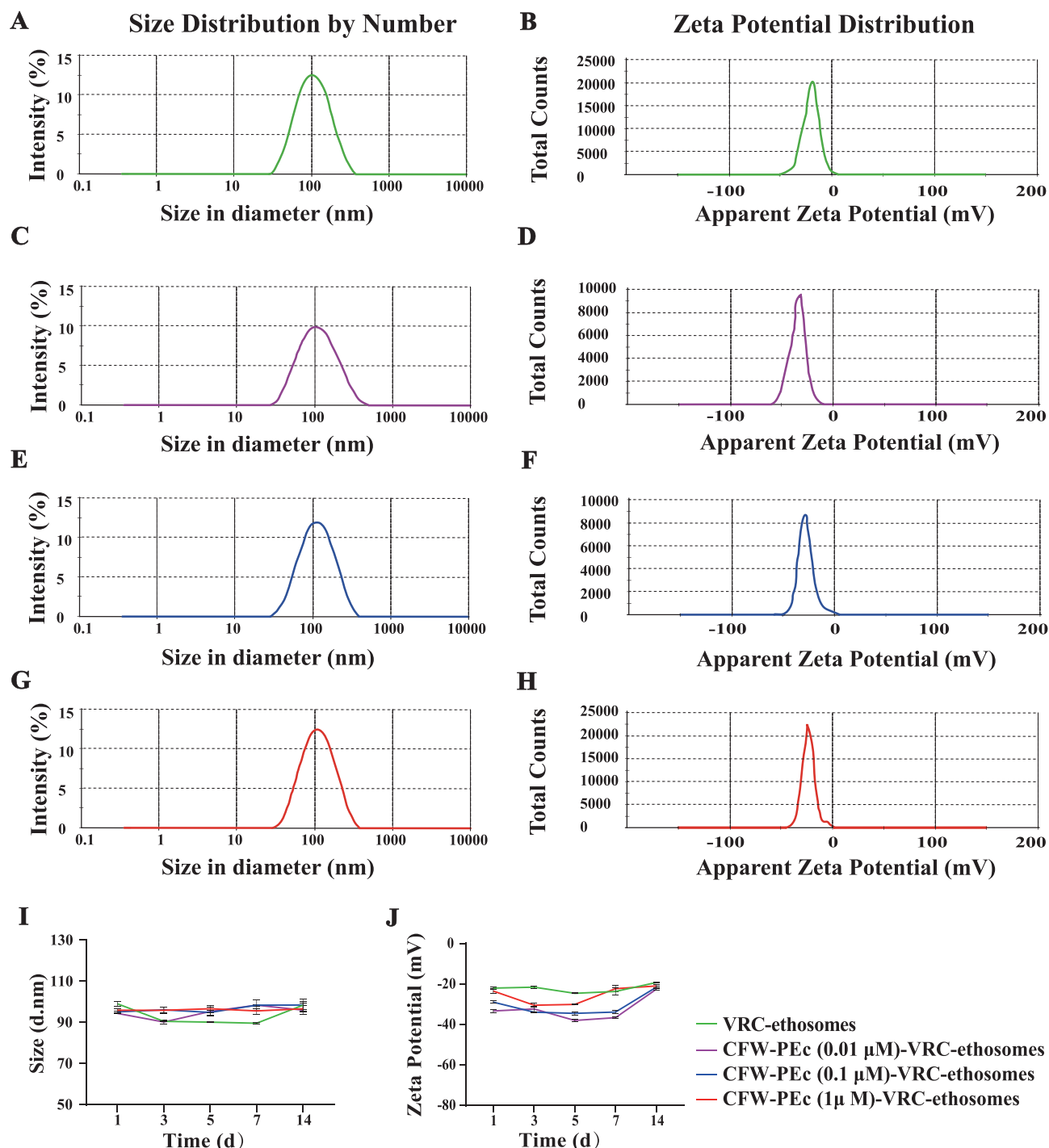


Figure 3 (A–H) Comparative analysis illustrating zeta potential and particle size distribution of VRC-ethosomes (green), CFW-PEc (0.01 μ M)-VRC-ethosomes (purple), CFW-PEc (0.1 μ M)-VRC-ethosomes (blue), and CFW-PEc (1 μ M)-VRC-ethosomes (red), highlighting the differences in their drug delivery profiles. **(I–J)** Stability assessment of CFW-PEc (0.01 μ M–1 μ M)-VRC-ethosomes showing no significant changes in particle size and zeta potential after 2 weeks at 25°C, suggesting robust storage conditions.

An *in vitro* cytotoxicity assay was conducted to evaluate the safety profile of CFW-PEc (0.01–1 μ M)-ethosomes and CFW-PEc (0.01–1 μ M)-VRC (0.5 μ g/mL)-ethosomes in mammalian cells. The cell viability of 293T cells exposed to the tested components was compared to that of cells treated with a PBS solution, as illustrated in **Figure 4B**. Notably, the cell viability of the 293T cells treated with CFW-PEc (0.01–1 μ M)-ethosomes exceeded 93%, while a slight decrease to approximately 88% was observed in groups treated with CFW-PEc (0.01–1 μ M)-VRC (0.5 μ g/mL)-ethosomes, likely due

Table 1 Therapeutic Properties of Nanoparticles (n = 3)

	CFW-PEc (0.01 μ M)-VRC-Ethosomes	CFW-PEc (0.1 μ M)-VRC-Ethosomes	CFW-PEc (1 μ M)-VRC-Ethosomes	VRC-Ethosomes
Size (nm)	94.32 \pm 0.045	95.08 \pm 0.28	95.93 \pm 0.63	98.63 \pm 1.19
Zeta Potential (mV)	-33.1 \pm 0.7	-28.9 \pm 0.6	-23.25 \pm 1.05	-21.9 \pm 0.4
Encapsulation efficiency (%)	39.20 \pm 0.96	43.27 \pm 0.07	43.67 \pm 2.15	53.35 \pm 0.51
Drug loading capacity (%)	4.78 \pm 0.12	5.32 \pm 0.09	5.33 \pm 0.26	6.51 \pm 0.06

Note: All data expressed as means \pm standard deviations.

Abbreviations: EE, Entrapment efficiency; DL, Drug loading capacity.

to the presence of VRC. These results indicate that CFW-PEc (0.01–1 μ M)-ethosomes demonstrate a favorable safety profile in the context of VRC drug delivery *in vitro*. The favorable safety profile demonstrated by CFW-PEc in mammalian cell assays suggests reduced cytotoxicity of CFW-PEc-VRC-ethosomes compared to previously developed nanoparticle systems, which often induce adverse effects at therapeutic doses.^{52,53} Such profiles are crucial for maintaining patient safety and compliance during treatment.

Cellular Uptake of CFW-PEc-C6-Ethosomes in *C. albicans* Yeast Cells

The photoluminescence of C6 is commonly utilized to analyze the cellular uptake of non-fluorescent drug molecules using fluorescence microscopy.^{54,55} To assess the impact of CFW-PEc on nanoparticle drug delivery effectiveness, the intracellular uptake of CFW-PEc (0.01–1 μ M)-C6-ethosomes and C6-ethosomes was quantitatively evaluated in *C. albicans* yeast cells through confocal microscopy. Figure 5A–D display confocal micrographs depicting the uptake of C6-loaded ethosomes into *C. albicans* yeast cells. In the groups treated with CFW-PEc (0.01 μ M)-C6-ethosomes (Figure 5A), the fluorescence intensity of C6 peaked at 3 hours and subsequently exhibited a rapid decline at 6 and 9 hours. The fluorescence intensity of CFW-PEc (0.1 μ M)-C6-ethosomes (Figure 5B) reached its maximum at 6 hours and remained stable until 9 hours. For the groups treated with CFW-PEc (1 μ M)-C6-ethosomes (Figure 5C), the fluorescence intensity peaked at 6 hours before undergoing a rapid decrease at 9 hours. Interestingly, the peak fluorescence intensity of the three distinct CFW-PEc-C6-ethosomes formulations was observed at 6 hours in the groups treated with CFW-PEc (0.1 μ M)-C6-ethosomes. The treatment with C6-ethosomes showed a fluorescence intensity trend similar to that of the groups treated with CFW-PEc (0.01 μ M)-C6-ethosomes (Figure 5D). These results indicate a difference in nanoparticle uptake rates between CFW-PEc-C6-ethosomes and C6-ethosomes. The inclusion of CFW-PEc has a notable impact on the uptake of ethosomes in *C. albicans* yeast cells.

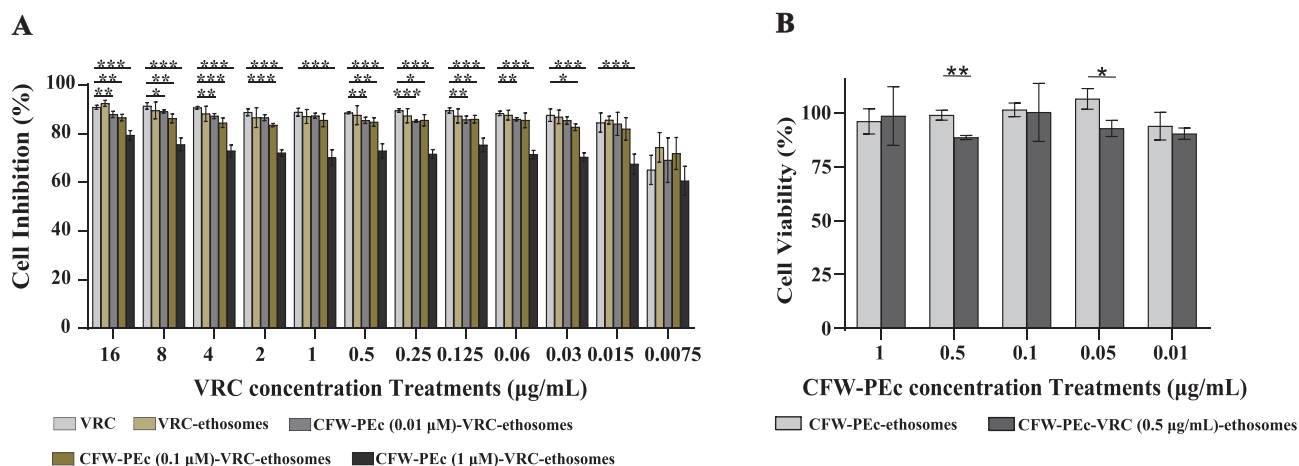


Figure 4 (A) *In vitro* antifungal activity of CFW-PEc (0.01–1 μ M)-VRC-ethosomes, VRC-ethosomes, and VRC against *C. albicans* yeast cells, emphasizing significant antifungal efficacy (* $P \leq 0.05$; ** $P \leq 0.01$; *** $P \leq 0.001$). **(B)** Cytotoxicity assessment of CFW-PEc formulations on 293T cells, reinforcing safety profiles with significant differences noted at various concentrations (* $P \leq 0.05$; ** $P \leq 0.01$).

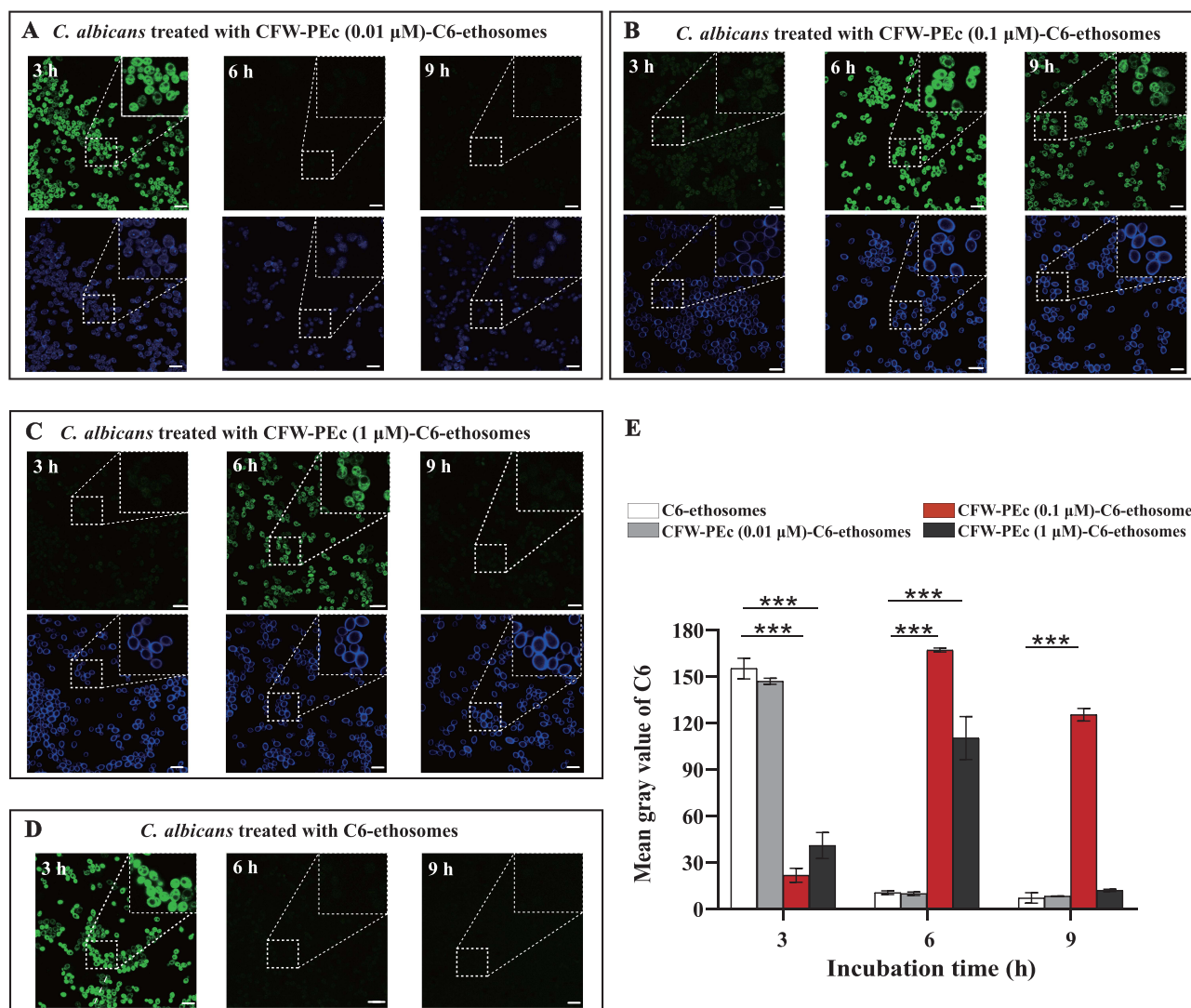


Figure 5 (A–D) Confocal microscopy images show the uptake of CFW-PEc (0.01 μ M)-C6-ethosomes, CFW-PEc (0.1 μ M)-C6-ethosomes, CFW-PEc (1 μ M)-C6-ethosomes, and C6-ethosomes in *C. albicans* yeast cells over time (3, 6, and 9 hours). The peak fluorescence intensity of C6 (green) detected at various time points indicates differences in uptake efficiency influenced by CFW-PEc, while the blue fluorescence originates from CFW-PEc excitation, illustrating its distribution within the cells. All images include scale bars of 10 μ m, with magnified regions outlined by white dashed lines for clarity. **(E)** Quantification of fluorescence intensity for C6-loaded nanoparticles, showing significant differences in uptake efficiency with the highest mean gray value for CFW-PEc (0.1 μ M)-C6-ethosomes at 6 hours compared to C6-ethosomes (***) ($P \leq 0.001$).

Furthermore, the fluorescence intensity in the cellular uptake of dye-loaded nanoparticles was quantified as the mean gray value using ImageJ (Figure 5E). The mean gray value in the cellular uptake of CFW-PEc (0.1 μ M)-C6-ethosomes reached the maximum value at 6 hours, showing a slight increase compared to the uptake of C6-ethosomes at 3 hours. The value in groups treated with CFW-PEc (0.1 μ M)-C6-ethosomes showed the lowest level at 3 hours compared to all other groups. However, at 9 hours, it was only approximately 30% lower than the maximum value. Our results indicated that CFW-PEc could prolong the nanoparticle uptake in *C. albicans* yeast cells through the positive interaction between CFW-PEc and chitin present in the cell wall. The concentration of CFW-PEc within the nanoparticles is likely to be a critical factor in influencing the strength of the nanoparticles during their interaction with chitin in the cell wall of *C. albicans*. Consequently, optimizing the amount of CFW-PEc can enhance the effectiveness of nanoparticle drug delivery in *C. albicans* yeast cells.

Cellular Uptake of CFW-PEc-C6-Ethosomes in *C. albicans* Hyphal Cells

C. albicans demonstrates the ability to grow as budding yeast or filamentous pseudohyphal and hyphal forms in response to environmental cues, impacting its virulence. The transformation from yeast to hypha enables the fungus to evade macrophage phagocytosis, increasing the likelihood of tissue invasion and damage in the host.⁵⁶ The impact of CFW-PEc on nanoparticle drug delivery effectiveness was assessed by quantitatively evaluating the intracellular uptake of CFW-PEc (0.01–1 μ M)-C6-ethosomes and C6-ethosomes in *C. albicans* hyphal cells using confocal microscopy. Figure 6A–D depict confocal micrographs illustrating the uptake of C6-loaded ethosomes into *C. albicans* hyphal cells, where the fluorescence intensity of C6 notably decreased. In contrast to *C. albicans* yeast cells treated with CFW-PEc (0.01 μ M)-C6-ethosomes, the fluorescence intensity of C6 peaked at 6 hours and persisted until 9 hours (Figure 6A). The peak fluorescence intensity of C6 in groups treated with CFW-PEc (0.1 μ M)-C6-ethosomes (Figure 6B) occurred at 6 hours and remained stable until 9 hours, significantly surpassing other groups. The fluorescence intensity profile of C6 in groups treated with CFW-PEc (1 μ M)-C6-ethosomes closely mirrored that of the groups treated with CFW-PEc (0.01 μ M)-C6-ethosomes (Figure 6C). In C6-ethosomes treated groups (Figure 6D), the fluorescence intensity of C6 was nearly undetectable after 6 hours. The results suggest that the uptake of C6-loaded ethosomes into *C. albicans* hyphal cells is influenced by the amount of CFW-PEc. Different fluorescence intensity patterns were observed in hyphal cells treated with various formulations. The highest fluorescence intensity of C6 was observed in cells treated with CFW-PEc (0.1 μ M)-C6-ethosomes, indicating enhanced uptake effectiveness.

Moreover, the fluorescence intensity associated with the cellular internalization of C6-loaded nanoparticles in *C. albicans* hyphal cells was quantified as the mean gray value utilizing ImageJ (Figure 6E). In *C. albicans* hyphal cells, the mean gray value for the cellular uptake of CFW-PEc (0.1 μ M)-C6-ethosomes was 1.21 times higher at 6 hours compared to C6-ethosomes at 3 hours, and it was only approximately 35% lower than the maximum value at 9 hours. Notably, at various time points, the mean gray value for the cellular uptake of CFW-PEc (0.1 μ M) was significantly greater than other CFW-PEc-C6-ethosomes formulations. Importantly, when comparing with Figure 5E, the mean gray value for the cellular uptake of CFW-PEc (0.1 μ M)-C6-ethosomes in *C. albicans* yeast cells at 6 hours was 1.24 times higher than in hyphal cells. Quantitative analysis revealed an increased cellular uptake of CFW-PEc (0.1 μ M)-C6-ethosomes at 6 and 9 hours compared to C6-ethosomes in hyphal cells. Additionally, the uptake of CFW-PEc (0.1 μ M) was consistently higher than other formulations. The comparison with yeast cells highlighted a significant difference in nanoparticle uptake between hyphal and yeast cells, emphasizing the potential impact of cell type on the efficiency of uptake.

Hyphae play a crucial role in the development and structural integrity of *C. albicans* biofilms, serving as a support scaffold for various cell types within the biofilm. The ability to form and adhere to hyphae is essential for the normal development and maintenance of biofilms, highlighting their importance in biofilm architecture and stability.⁵⁷ A crystal violet method was performed to evaluate the antifungal activity of CFW-PEc (0.01–1 μ M)-VRC-ethosomes against *C. albicans* hyphal cells. The results summarized in Figure 6F. In groups treated with CFW-PEc (0.1 μ M)-VRC-ethosomes at 8 μ g/mL, the inhibition rate of biofilm formation in *C. albicans* hyphal cells reached approximately 82%, surpassing that of other groups. Even at 4 μ g/mL, the inhibition rate still maintained the superiority. These results indicate that CFW-PEc-VRC-ethosomes may be effective in preventing the development and stability of *C. albicans* biofilms, highlighting their potential as a treatment for *C. albicans* infections. This improvement may be attributed to the enhanced uptake effectiveness of CFW-PEc-VRC-ethosomes in *C. albicans* hyphal cells.

Fluorescence Imaging of CFW-PEc-Cy5.5-Ethosomes in vivo

Cyanine-based systems play a crucial role in providing essential information for biomedical research in live animal imaging, owing to their appealing optical properties and suitable bio-functionality.^{58,59} To investigate the accumulation property of CFW-PEc-ethosomes in mice, Cy5.5-ethosomes, and CFW-PEc (0.01–1 μ M)-Cy5.5-ethosomes were prepared. The experimental procedure is depicted in Figure 7A. An intraperitoneal infection model was established in Kunming mice infected with *C. albicans* yeast cells. Seven days post-infection, mice were intravenously administered

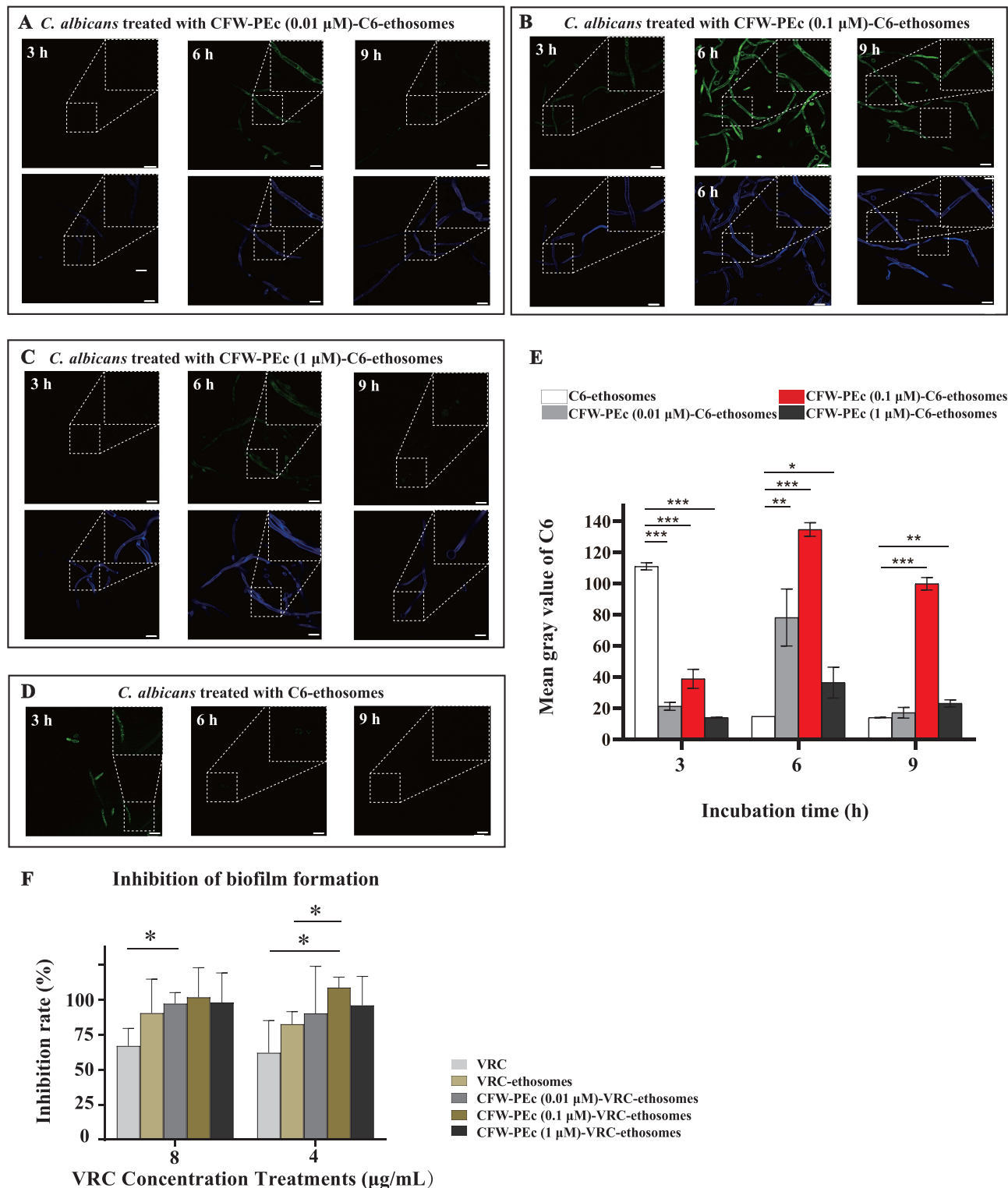


Figure 6 (A–D) Confocal microscopy images illustrating the uptake of CFW-PEc (0.01 μ M)-C6-ethosomes, CFW-PEc (0.1 μ M)-C6-ethosomes, CFW-PEc (1 μ M)-C6-ethosomes, and C6-ethosomes in *C. albicans* hyphal cells over 3, 6, and 9 hours in spider medium. The images display dual fluorescence channels, with green fluorescence representing C6 uptake and blue fluorescence indicating the distribution of CFW-PEc within the cells. All images include scale bars of 10 μ m, with white dashed lines outlining magnified regions for clarity. **(E)** Quantification of fluorescence intensity for C6-loaded nanoparticles, showing significant differences in uptake efficiency with the highest mean gray value for CFW-PEc (0.1 μ M)-C6-ethosomes at 6 hours compared to C6-ethosomes (* $P \leq 0.05$; ** $P \leq 0.01$; *** $P \leq 0.001$). **(F)** Results of the crystal violet assay demonstrating the inhibition rate of biofilm formation in *C. albicans* hyphal cells treated with CFW-PEc (0.1 μ M)-VRC-ethosomes at 4 and 8 μ g/mL, highlighting significant efficacy in biofilm inhibition (* $P \leq 0.05$).

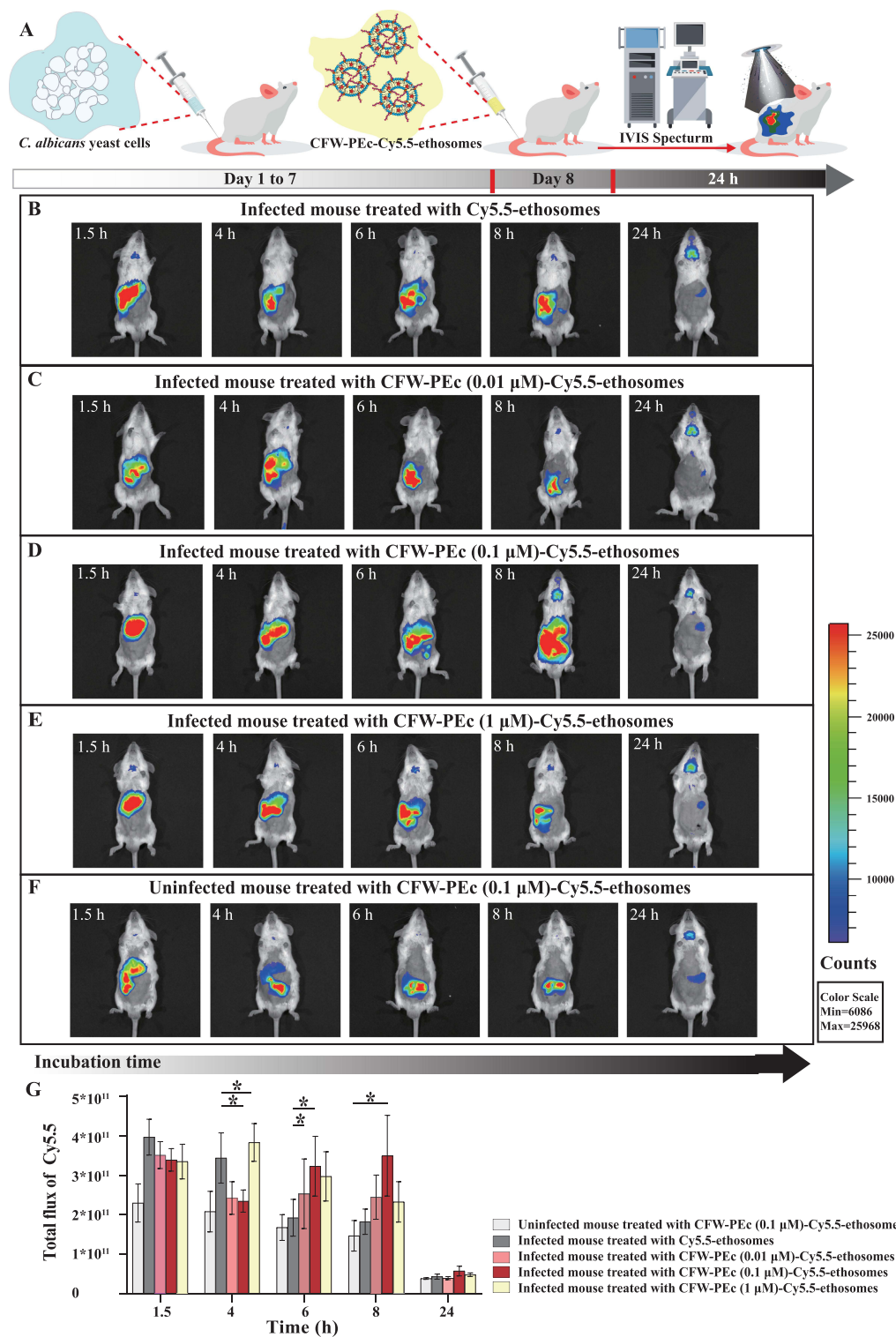


Figure 7 (A) Schematic representation of the experimental procedure for in vivo fluorescence imaging of Cy5.5-loaded nanoparticles in Kunming mice. (B–F) Fluorescence imaging results at various time points post-treatment using an IVIS Spectrum. Each group of four infected Kunming mice received intravenous treatments with different formulations of fluorescent nanoparticles, and their fluorescence was assessed at five different time points. (B) Fluorescence imaging of infected mice treated with Cy5.5-ethosomes, showing strong fluorescence signals in the peritoneal cavity after 1.5 hours. (C) Infected mice treated with CFW-PEc (0.01 μ M)-Cy5.5-ethosomes exhibited enhanced fluorescence retention. (D) Infected mice treated with CFW-PEc (0.1 μ M)-Cy5.5-ethosomes demonstrated significant fluorescence accumulation, especially at 8 hours. (E) Infected mice treated with CFW-PEc (1 μ M)-Cy5.5-ethosomes also showed improved signal retention. (F) Non-infected mice treated with CFW-PEc (0.1 μ M)-Cy5.5-ethosomes presented lower fluorescence levels across all time points, indicating reduced non-specific accumulation. (G) Analysis using Living Image software, demonstrating that the total flux of Cy5.5 was significantly higher in infected mice treated with CFW-PEc formulations compared to Cy5.5-ethosomes alone (* $P \leq 0.05$).

Cy5.5 in various formulations, followed by a live animal imaging assay to monitor the real-time fluorescence signals of CFW-PEc (0.01–1 μM)-Cy5.5-ethosomes and Cy5.5-ethosomes.

Figure 7B illustrates that infected mice treated with Cy5.5-ethosomes exhibited consistent and intense signals in the peritoneal cavity after 1.5 hours. The fluorescence intensity gradually decreased over time, maintaining a moderate level after 8 hours, and becoming barely detectable after 24 hours. In comparison, the fluorescence patterns in mice treated with CFW-PEc (0.01–1 μM)-Cy5.5-ethosomes (Figure 7C–E) were different from those treated with Cy5.5-ethosomes, with the former group showing relatively higher fluorescence levels between 6 and 8 hours. Notably, at 8 hours, the fluorescence intensity of Cy5.5 in the CFW-PEc (0.1 μM)-Cy5.5-ethosomes group was significantly stronger, and the area distribution was larger compared to those in the Cy5.5-ethosomes group (Figure 7D). These findings indicate that Cy5.5-loaded nanoparticles can be delivered intravenously into the peritoneal cavity, with CFW-PEc (0.1 μM)-Cy5.5-ethosomes exhibiting significantly longer half-lives in infected tissues in mice. In order to address the potential non-specific binding of CFW-PEc-ethosomes in the host, uninfected mice were administered treatment with CFW-PEc (0.1 μM)-Cy5.5-ethosomes. Figure 7F illustrates the detection of fluorescence signals in the peritoneal cavity of uninfected mice after 1.5 hours, with consistently lower Cy5.5 signals observed at all time points. These results suggest that CFW-PEc (0.1 μM)-Cy5.5-ethosomes could be subject to relatively rapid metabolism in uninfected mice, potentially reducing the likelihood of non-specific interactions. This contrasts sharply with conventional nanoparticle formulations, such as poly(lactic-co-glycolic acid) and inorganic nanoparticles that may often experience rapid clearance and non-specific accumulation, limiting their clinical utility.^{60,61} The improvement in efficacy is closely related to the extended circulation time in the bloodstream and the high accumulation at the site of fungal infection.⁶²

Analysis using the Living Image software (Figure 7G) demonstrated that mice infected with Cy5.5-ethosomes maintained a total flux of Cy5.5 at around 3.97×10^{11} after 1.5 hours, showing a slight increase (1.11-fold to 1.18-fold) compared to the three groups treated with CFW-PEc (0.01–1 μM)-Cy5.5-ethosomes. However, the total flux of Cy5.5 in infected mice treated with CFW-PEc (0.1 μM)-Cy5.5-ethosomes was notably 1.68-fold higher than in those treated with Cy5.5-ethosomes at 6 hours, and substantially 1.91-fold higher than in those treated with Cy5.5-ethosomes at 8 hours. Collectively, the results suggest that CFW-PEc (0.1 μM)-Cy5.5-ethosomes demonstrate enhanced accumulation and prolonged half-lives in infected tissues in mice compared to Cy5.5-ethosomes alone, potentially indicating their effectiveness for targeted drug delivery. This improved performance is likely due to the active targeting ability of CFW-PEc, which facilitates nanoparticle accumulation in fungal infection sites through blood circulation. The improved effectiveness of drug delivery suggests that antifungal drug-loaded CFW-PEc-ethosomes may have promising therapeutic benefits for treating *C. albicans* infections in vivo.

Antifungal Activity of CFW-PEc-VRC-Ethosomes in vivo

The antifungal efficacy of CFW-PEc-VRC-ethosomes was assessed by administering 2 mg/kg VRC in different formulations to five groups of Kunming mice infected by *C. albicans* via intraperitoneal injection once daily for seven consecutive days. The control group received appropriate PBS treatment. After 8 days post-infection, the liver and kidney tissues of the mice were homogenized to quantify CFU. The experimental procedure is illustrated in Figure 8A. The results are summarized in Figure 8B and C. Compared to the control group, there was a noticeable trend of decreased fungal burdens in the liver and kidney of groups treated with both VRC and VRC-ethosomes. The number of CFU counts in the groups treated with VRC-ethosomes was only 3.3-fold lower than that of the control group in the kidney and approximately 44% lower in the liver, likely due to limitations in treatment duration and dosage. A greater drop in CFU counts was observed in the three groups treated with CFW-PEc (0.01–1 μM)-VRC-ethosomes. Specifically, the CFW-PEc (0.1 μM)-VRC-ethosomes group showed significantly lower CFU counts in the liver and kidney compared to the VRC-ethosomes group, with a 5-fold reduction in the liver and a 7.8-fold reduction in the kidney.

The histopathological analysis was performed to assess the therapeutic efficacy of drug treatment in five groups. Liver and kidney sections were stained with hematoxylin and eosin (H&E) and are captured in Figure 8D–O. Figure 8D shows that *C. albicans* infection in the control group induced a necrotic lesion in the liver with a significant level of neutrophil infiltration. In contrast, Figure 8E and F demonstrate a more pronounced necrotic lesion with visible necrotic tissue in the center in the groups treated with both VRC and VRC-ethosomes. The necrotic lesion in the groups treated with CFW-PEc

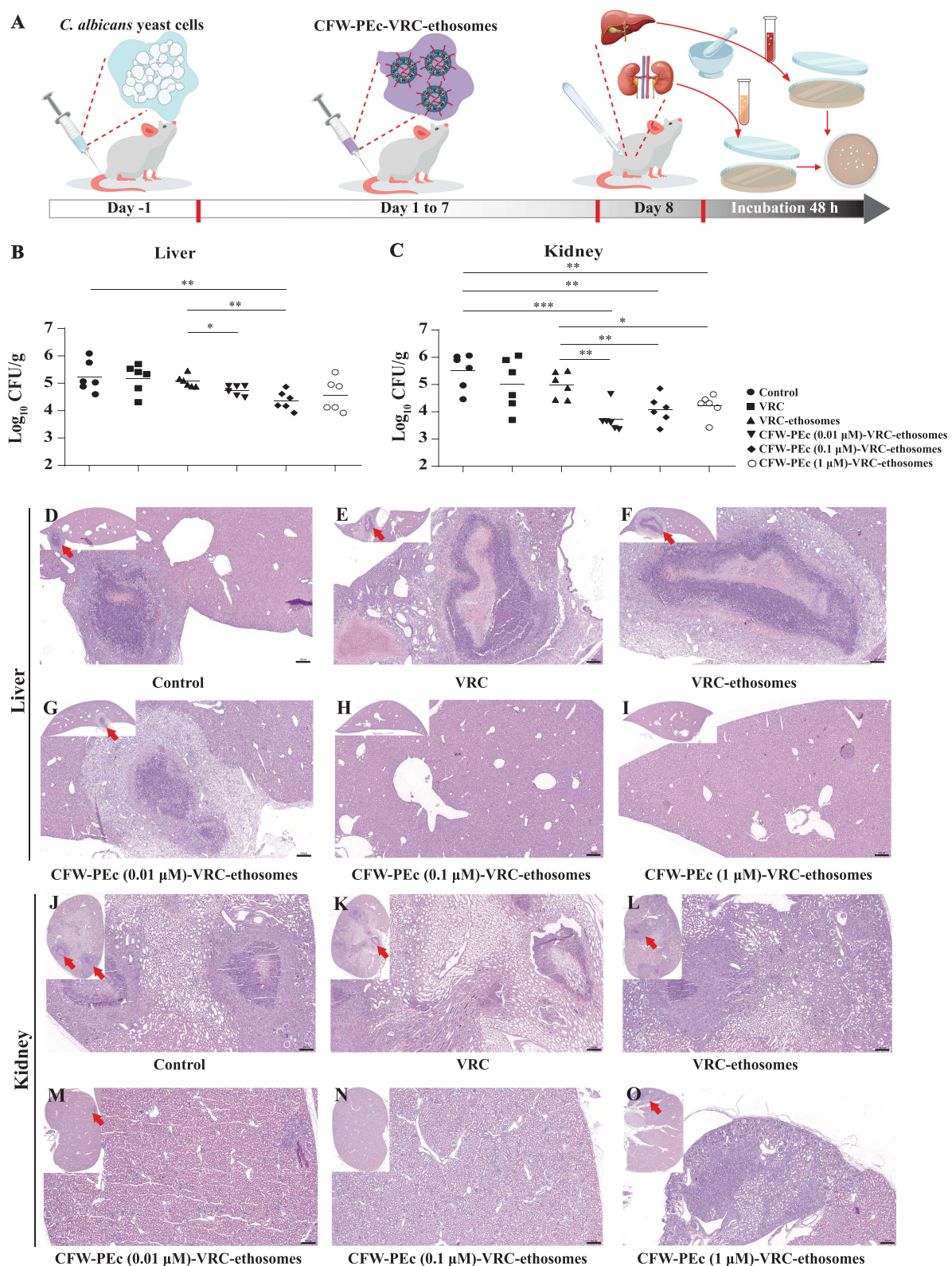


Figure 8 In vivo assessment of the antifungal activity of CFW-PEc-VRC-ethosomes in Kunming mice infected with *C. albicans*. **(A)** Schematic representation of the experimental procedure illustrating the treatment protocol. **(B and C)** Quantification of CFUs from liver **(B)** and kidney **(C)** tissues of infected mice treated with various formulations, showing significantly lower fungal burdens in those receiving CFW-PEc-VRC-ethosomes compared to the controls (* $P \leq 0.05$; ** $P \leq 0.01$; *** $P \leq 0.001$). **(D–I)** Histopathological analysis of liver sections stained with H&E, showing varying degrees of necrotic lesions and inflammatory responses in the control and treated groups. Notably, CFW-PEc (0.1 μM)-VRC-ethosomes exhibited minimal pathological changes compared to controls. **(J–O)** Histopathological analysis of kidney tissues indicating inflammation and damage due to *C. albicans* infection; the treated groups displayed improved tissue integrity. Red arrows highlight pathological changes in liver and kidney indicative of *C. albicans* infection. All images include scale bars of 200 μm.

(0.01 μM)-VRC-ethosomes, as shown in Figure 8G, displayed substantial infiltration of inflammatory cells, surrounded by granulation tissue but devoid of discernible necrotic tissue. Conversely, Figure 8H and I show no notable pathological changes resulting from *C. albicans* infection in the groups treated with CFW-PEc (0.1 μM)-VRC-ethosomes and CFW-PEc (1 μM)-VRC-ethosomes. Figure 8J illustrates that *C. albicans* infection in the control groups led to a necrotic lesion in the kidney with a high level of neutrophil infiltration and visible necrotic tissue in the center, similar to the VRC-treated groups shown in Figure 8K. Furthermore, Figure 8L depicts abscess formation due to *C. albicans* infection with neutrophil infiltration in the groups treated with VRC-ethosomes. Figure 8M shows localized interstitial infiltration of inflammatory cells in the groups treated with CFW-PEc (0.01 μM)-VRC-ethosomes. Notably, Figure 8N indicates no significant pathological changes due to *C. albicans* infection in the groups treated with CFW-PEc (0.1 μM)-VRC-ethosomes. Figure 8O illustrates a significant inflammatory response with a large number of inflammatory cells infiltrating the diffuse interstitium in the groups treated with CFW-PEc (1 μM)-VRC-ethosomes. Unlike existing antifungal therapies that often have broad, non-specific action, CFW-PEc leverages chitin's unique presence in fungal cell walls to enhance specificity. This targeted approach reduces collateral damage to host tissues and improves patient tolerance, which is a commonly recognized drawback in traditional antifungal therapies.^{63,64}

The results suggest that the antifungal efficacy of CFW-PEc-VRC-ethosomes was evaluated in mice infected with *C. albicans*. Treatment with VRC and VRC-ethosomes led to decreased fungal burdens in the liver and kidney compared to the control group, although the reduction was more pronounced in both organs. Furthermore, groups treated with CFW-PEc (0.01–1 μM)-VRC-ethosomes exhibited a greater decrease in CFU counts. Histopathological analysis revealed varying degrees of necrotic lesions and inflammatory responses in the liver and kidney, with notable improvements in groups treated with CFW-PEc (0.1 μM)-VRC-ethosomes, indicating a potential therapeutic benefit of this formulation in *C. albicans* infection. While typical nanoparticle-loaded antifungal drugs, such as VRC-ethosomes, may exhibit a certain level of effectiveness, the synergy between CFW-PEc and the ethosomal delivery system leads to a more potent therapeutic outcome, as illustrated by the observed reductions in fungal burden and favorable histopathological findings. The specific binding of CFW-PEc to *C. albicans* cells facilitates the accumulation of VRC-loaded nanoparticles at the infection sites through the bloodstream, thereby augmenting the antifungal efficacy of CFW-PEc-VRC-ethosomes. Furthermore, the in vivo evaluation of CFW-PEc-VRC-ethosomes confirms their safety profile, suggesting the potential of nanoparticle-based drug therapy, offering benefits like improved solubility and extended half-life.

The CFW-PEc drug delivery system demonstrated in this study has profound clinical significance, particularly in its application for antifungal therapy in immunocompromised patients. By targeting the unique chitin present in fungal cell walls, the high specificity of CFW-PEc not only enhances the antifungal activity of the drug but also significantly reduces potential toxicity to normal cells. This selective targeted drug delivery system may lower treatment costs by improving drug efficacy and reducing the occurrence of resistance issues, thereby decreasing the overall treatment burden on patients. Furthermore, the results of this study indicate that CFW-PEc-VRC-ethosomes significantly reduced the fungal burden in the liver and kidneys of infected mice, suggesting that this approach could improve patient outcomes and quality of life in a clinical context. For high-risk groups, especially those undergoing chemotherapy or organ transplantation, CFW-PEc may change the landscape of antifungal therapy by reducing systemic side effects and enhancing efficacy. Therefore, future clinical trials are necessary to validate the effectiveness and safety of this system, paving the way for its application in clinical practice.

Conclusion

Our study on the synthesis, characterization, and application of CFW-PEc and its nanoparticle formulations (CFW-PEc-VRC-ethosomes) has demonstrated significant findings in the field of antifungal therapy. The successful synthesis of CFW-PEc was confirmed through NMR spectroscopy, showing complete linkage between CFW and PE. The specific binding of CFW-PEc to chitin in fungal cell walls was established, distinguishing it from mammalian cells and emphasizing its specificity and potential for targeted fungal therapy. In vitro and in vivo assays highlighted the effective antifungal activity of CFW-PEc and its enhanced efficacy when used in nanoparticle formulations. The VRC-loaded CFW-PEc-ethosomes showed concentration-dependent inhibition of *C. albicans*, with excellent safety profiles in mammalian cells. Notably, the inclusion of CFW-PEc in ethosomes did not significantly alter the particle size or zeta

potential but enhanced the drug delivery efficiency through improved stability and cellular uptake, particularly in fungal cells. This role of CFW-PEc in facilitating targeted delivery was further corroborated by live animal imaging, demonstrating prolonged retention and higher fluorescence intensity of CFW-PEc-Cy5.5-ethosomes in infected tissues. Moreover, the therapeutic efficacy of CFW-PEc-VRC-ethosomes was validated through a decrease in fungal burden and improved histopathological outcomes in infected mice, showcasing a significant reduction in necrotic lesions and inflammatory responses.

In light of these findings, the clinical relevance of CFW-PEc-VRC-ethosomes extends beyond the laboratory, presenting a potentially transformative approach to antifungal therapy in clinical settings. Future research should focus on conducting clinical trials to evaluate the effectiveness of CFW-PEc-based formulations in diverse patient populations and to explore possible combination therapies with existing antifungal agents to enhance therapeutic outcomes. Additionally, investigating the long-term effects and potential resistance mechanisms associated with CFW-PEc will be critical for its success as a novel antifungal treatment. By enhancing our knowledge of the pharmacokinetics and pharmacodynamics of CFW-PEc, we can facilitate the development of novel approaches to tackle difficult fungal infections and enhance patient outcomes. This approach could potentially revolutionize the treatment of fungal infections, offering a more effective, targeted, and safer therapeutic option compared to traditional antifungal treatments.

Ethics

All experiments related with human cells were approved by the Research Ethics Committees of Binzhou Medical University (Approval No. 2024-118). The 293T and MDA-MB-231 cell lines were authenticated using an STR profile, which was performed by Shanghai Biowing Applied Biotechnology Co., Ltd. All animal experiments were conducted in accordance with the guidelines outlined in NIH Publications No. 8023, revised in 1978, and were approved by the Research Ethics Committees of Binzhou Medical University (Approval No. 2024-209). The Chinese National Guidelines (GB/T 35892-2018) were followed for the ethical review of laboratory animal welfare.

Author Contributions

These authors contributed equally and shared co-first authorship: Ting Shen, Mengxin Li, and Baocheng Tian. All authors made a significant contribution to the work reported, whether that is in the conception, study design, execution, acquisition of data, analysis and interpretation, or in all these areas; took part in drafting, revising, or critically reviewing the article; gave final approval of the version to be published; have agreed on the journal to which the article has been submitted; and agree to be accountable for all aspects of the work.

Funding

This work was financially supported by the National Natural Science Foundation of China (81501784, 81703717, and 32270205).

Disclosure

The authors report no conflicts of interest in this work.

References

1. Lockhart SR, Guarner J. Emerging and reemerging fungal infections. *Semin Diagn Pathol.* 2019;36(3):177–181. doi:10.1053/j.semdp.2019.04.010
2. Lakoh S, Rickman H, Sesay M, et al. Prevalence and mortality of cryptococcal disease in adults with advanced HIV in an urban tertiary hospital in Sierra Leone: a prospective study. *BMC Infect Dis.* 2020;20(1):141. doi:10.1186/s12879-020-4862-x
3. Otto WR, Green AM. Fungal infections in children with haematologic malignancies and stem cell transplant recipients. *Br J Haematol.* 2020;189(4):607–624. doi:10.1111/bjh.16452
4. Gushiken AC, Saharia KK, Baddley JW. Cryptococcosis. *Infect Dis Clin North Am.* 2021;35(2):493–514. doi:10.1016/j.idc.2021.03.012
5. Blot S, Rello J, Koulenti D. Diagnosing invasive pulmonary aspergillosis in ICU patients: putting the puzzle together. *Curr Opin Crit Care.* 2019;25(5):430–437. doi:10.1097/MCC.0000000000000637
6. Hadrich I, Ayadi A. Epidemiology of antifungal susceptibility: review of literature. *J Mycol Med.* 2018;28(3):574–584. doi:10.1016/j.mycmed.2018.04.011

7. Talapko J, Juzbasic M, Matijevic T, et al. *Candida albicans*-the virulence factors and clinical manifestations of infection. *J Fungi*. 2021;7(2):79. doi:10.3390/jof7020079
8. Noble SM, Gianetti BA, Witchley JN. *Candida albicans* cell-type switching and functional plasticity in the mammalian host. *Nat Rev Microbiol*. 2017;15(2):96–108. doi:10.1038/nrmicro.2016.157
9. Prasad P, Tippana M. Morphogenic plasticity: the pathogenic attribute of *Candida albicans*. *Curr Genet*. 2023;69(2–3):77–89. doi:10.1007/s00294-023-01263-5
10. Revie NM, Iyer KR, Robbins N, Cowen LE. Antifungal drug resistance: evolution, mechanisms and impact. *Curr Opin Microbiol*. 2018;45:70–76. doi:10.1016/j.mib.2018.02.005
11. Johnson LB, Kauffman CA. Voriconazole: a new triazole antifungal agent. *Clin Infect Dis*. 2003;36(5):630–637. doi:10.1086/367933
12. Jeu L, Piacenti FJ, Lyakhovetskiy AG, Fung HB. Voriconazole. *Clin Ther*. 2003;25(5):1321–1381. doi:10.1016/S0149-2918(03)80126-1
13. Job KM, Olson J, Stockmann C, et al. Pharmacodynamic studies of voriconazole: informing the clinical management of invasive fungal infections. *Expert Rev Anti Infect Ther*. 2016;14(8):731–746. doi:10.1080/14787210.2016.1207526
14. Collins LM, Moore R, Sobel JD. Prognosis and long-term outcome of women with idiopathic recurrent vulvovaginal candidiasis caused by *Candida albicans*. *J Low Genit Tract Dis*. 2020;24(1):48–52. doi:10.1097/LGT.0000000000000496
15. Perez-Pitarch A, Guglieri-Lopez B, Ferriols-Lisart R, et al. Pharmacokinetic/pharmacodynamic analysis of voriconazole against *Candida* spp. and *Aspergillus* spp. in allogeneic stem cell transplant recipients. *Ther Drug Monit*. 2019;41(6):740–747. doi:10.1097/FTD.0000000000000657
16. Cheng L, Xiang R, Liu F, et al. Therapeutic drug monitoring and safety of voriconazole in elderly patients. *Int Immunopharmacol*. 2020;78:106078. doi:10.1016/j.intimp.2019.106078
17. Zhong X, Tong X, Ju Y, Du X, Li Y. Interpersonal factors in the pharmacokinetics and pharmacodynamics of voriconazole: are CYP2C19 genotypes enough for us to make a clinical decision? *Curr Drug Metab*. 2018;19(14):1152–1158. doi:10.2174/1389200219666171227200547
18. Resztak M, Kosicka K, Zaleska P, Krawiec J, Glowka FK. Determination of total and free voriconazole in human plasma: application to pharmacokinetic study and therapeutic monitoring. *J Pharm Biomed Anal*. 2020;178:112952. doi:10.1016/j.jpba.2019.112952
19. Theuretzbacher U, Ihle F, Derendorf H. Pharmacokinetic/pharmacodynamic profile of voriconazole. *Clin Pharmacokinet*. 2006;45(7):649–663. doi:10.2165/00003088-200645070-00002
20. Levine MT, Chandrasekar PH. Adverse effects of voriconazole: over a decade of use. *Clin Transplant*. 2016;30(11):1377–1386. doi:10.1111/ctr.12834
21. Musayeva A, Riedl JC, Schuster AK, Wasielica-Poslednik J, Pfeiffer N, Gericke A. Topical voriconazole as supplemental treatment for acanthamoeba keratitis. *Cornea*. 2020;39(8):986–990. doi:10.1097/ICO.0000000000002315
22. Renzi DF, de Almeida Campos L, Miranda EH, et al. Nanoparticles as a tool for broadening antifungal activities. *Curr Med Chem*. 2021;28(9):1841–1873. doi:10.2174/0929867327666200330143338
23. Hindi KM, Ditto AJ, Panzner MJ, et al. The antimicrobial efficacy of sustained release silver-carbene complex-loaded L-tyrosine polyphosphate nanoparticles: characterization, in vitro and in vivo studies. *Biomaterials*. 2009;30(22):3771–3779. doi:10.1016/j.biomaterials.2009.03.044
24. Voltan AR, Quindos G, Alarcon KP, Fusco-Almeida AM, Mendes-Giannini MJ, Chorilli M. Fungal diseases: could nanostructured drug delivery systems be a novel paradigm for therapy? *Int J Nanomed*. 2016;11:3715–3730. doi:10.2147/IJN.S93105
25. Khan SH, Younus H, Allemailem KS, et al. Potential of methylglyoxal-conjugated chitosan nanoparticles in treatment of fluconazole-resistant *Candida albicans* infection in a murine model. *Int J Nanomed*. 2020;15:3681–3693. doi:10.2147/IJN.S249625
26. Moen MD, Lyseng-Williamson KA, Scott LJ. Liposomal amphotericin B: a review of its use as empirical therapy in febrile neutropenia and in the treatment of invasive fungal infections. *Drugs*. 2009;69(3):361–392. doi:10.2165/00003495-200969030-00010
27. Bekersky I, Fielding RM, Dressler DE, Lee JW, Buell DN, Walsh TJ. Pharmacokinetics, excretion, and mass balance of liposomal amphotericin B (AmBisome) and amphotericin B deoxycholate in humans. *Antimicrob Agents Chemother*. 2002;46(3):828–833. doi:10.1128/AAC.46.3.828-833.2002
28. Sim S, Wong NK. Nanotechnology and its use in imaging and drug delivery (Review). *Biomed Rep*. 2021;14(5):42. doi:10.3892/br.2021.1418
29. Patra JK, Das G, Fraceto LF, et al. Nano based drug delivery systems: recent developments and future prospects. *J Nanobiotechnol*. 2018;16(1):71. doi:10.1186/s12951-018-0392-8
30. Watkins R, Wu L, Zhang C, Davis RM, Xu B. Natural product-based nanomedicine: recent advances and issues. *Int J Nanomed*. 2015;10:6055–6074. doi:10.2147/IJN.S92162
31. Jafari A, Daneshamouz S, Ghasemiyeh P, Mohammadi-Samani S. Ethosomes as dermal/transdermal drug delivery systems: applications, preparation and characterization. *J Liposome Res*. 2023;33(1):34–52. doi:10.1080/08982104.2022.2085742
32. Gow NAR, Latge JP, Munro CA. The fungal cell wall: structure, biosynthesis, and function. *Microbiol Spectr*. 2017;5(3). doi:10.1128/microbiolspec.FUNK-0035-2016
33. Reese AJ, Yoneda A, Breger JA, et al. Loss of cell wall alpha(1-3) glucan affects *Cryptococcus neoformans* from ultrastructure to virulence. *Mol Microbiol*. 2007;63(5):1385–1398. doi:10.1111/j.1365-2958.2006.05551.x
34. Iorio E, Torosantucci A, Bromuro C, et al. *Candida albicans* cell wall comprises a branched beta-D-(1->6)-glucan with beta-D-(1->3)-side chains. *Carbohydr Res*. 2008;343(6):1050–1061. doi:10.1016/j.carres.2008.02.020
35. Latge JP. The cell wall: a carbohydrate armour for the fungal cell. *Mol Microbiol*. 2007;66(2):279–290. doi:10.1111/j.1365-2958.2007.05872.x
36. Wheeler RT, Kombe D, Agarwala SD, Fink GR. Dynamic, morphotype-specific *Candida albicans* beta-glucan exposure during infection and drug treatment. *PLoS Pathog*. 2008;4(12):e1000227. doi:10.1371/journal.ppat.1000227
37. Hejtmánek M, Doležel J, Holubová I. Staining of fungal cell walls with fluorescent brighteners: flow-cytometric analysis. *Folia Microbiol*. 1990;35(5):437–442. doi:10.1007/BF02821413
38. Ruchel R, Margraf S. Rapid microscopical diagnosis of deep-seated mycoses following maceration of fresh specimens and staining with optical brighteners. *Mycoses*. 1993;36(7–8):239–242. doi:10.1111/j.1439-0507.1993.tb00757.x
39. Monheit JE, Cowan DF, Moore DG. Rapid detection of fungi in tissues using calcofluor white and fluorescence microscopy. *Arch Pathol Lab Med*. 1984;108(8):616–618.
40. Roncero C, Valdivieso MH, Ribas JC, Duran A. Effect of calcofluor white on chitin synthases from *Saccharomyces cerevisiae*. *J Bacteriol*. 1988;170(4):1945–1949. doi:10.1128/jb.170.4.1945-1949.1988

41. Brasch J, Kreiselmaier I, Christophers E. Inhibition of dermatophytes by optical brighteners. *Mycoses*. 2003;46(3–4):120–125. doi:10.1046/j.1439-0507.2003.00857.x
42. Sadeghi G, Khaksar AA, Bassiri Jahromi S, et al. Fungistatic effects of optical brightener 220 against *Trichophyton tonsurans*, *Aspergillus fumigatus* and *Candida albicans*. *J Dermatol Treat*. 2009;20(2):120–123. doi:10.1080/09546630802449070
43. Shen T, Tian B, Liu W, et al. Transdermal administration of farnesol-ethosomes enhances the treatment of cutaneous candidiasis induced by *Candida albicans* in mice. *Microbiol Spectr*. 2024;12(4):e0424723. doi:10.1128/spectrum.04247-23
44. Soliman GM. Nanoparticles as safe and effective delivery systems of antifungal agents: achievements and challenges. *Int J Pharm*. 2017;523(1):15–32. doi:10.1016/j.ijpharm.2017.03.019
45. Walker LA, Munro CA, de Bruijn I, Lenardon MD, McKinnon A, Gow NA. Stimulation of chitin synthesis rescues *Candida albicans* from echinocandins. *PLoS Pathog*. 2008;4(4):e1000040. doi:10.1371/journal.ppat.1000040
46. Bowers B, Levin G, Cabib E. Effect of polyoxin D on chitin synthesis and septum formation in *Saccharomyces cerevisiae*. *J Bacteriol*. 1974;119(2):564–575. doi:10.1128/jb.119.2.564-575.1974
47. Singh P, Katkar K, Walski T, Bohara RA. Three in-one fenestrated approaches of yolk-shell, silver-silica nanoparticles: a comparative study of antibacterial, antifungal and anti-cancerous applications. *Heliyon*. 2023;9(8):e18034. doi:10.1016/j.heliyon.2023.e18034
48. Tran NT, Ha D, Pham LH, et al. Ag/SiO₂ nanoparticles stabilization with lignin derived from rice husk for antifungal and antibacterial activities. *Int J Biol Macromol*. 2023;230:123124. doi:10.1016/j.ijbiomac.2022.123124
49. Hernando S, Herran E, Figueiro-Silva J, et al. Intranasal administration of tat-conjugated lipid nanocarriers loading GDNF for Parkinson's disease. *Mol Neurobiol*. 2018;55(1):145–155. doi:10.1007/s12035-017-0728-7
50. de Sa FA, Taveira SF, Gelfuso GM, Lima EM, Gratieri T. Liposomal voriconazole (VOR) formulation for improved ocular delivery. *Colloids Surf B Biointerfaces*. 2015;133:331–338. doi:10.1016/j.colsurfb.2015.06.036
51. Zhang Z, Feng SS. The drug encapsulation efficiency, in vitro drug release, cellular uptake and cytotoxicity of paclitaxel-loaded poly(lactide)-tocopheryl polyethylene glycol succinate nanoparticles. *Biomaterials*. 2006;27(21):4025–4033. doi:10.1016/j.biomaterials.2006.03.006
52. Dupont B. Overview of the lipid formulations of amphotericin B. *J Antimicrob Chemother*. 2002;49 Suppl 1:31–36. doi:10.1093/jac/49.suppl_1.31
53. Laniado-Laborin R, Cabrales-Vargas MN. Amphotericin B: side effects and toxicity. *Rev Iberoam Micol*. 2009;26(4):223–227. doi:10.1016/j.riam.2009.06.003
54. Dong Y, Feng SS. In vitro and in vivo evaluation of methoxy polyethylene glycol-poly(lactide) (MPEG-PLA) nanoparticles for small-molecule drug chemotherapy. *Biomaterials*. 2007;28(28):4154–4160. doi:10.1016/j.biomaterials.2007.05.026
55. Yu C, He B, Xiong MH, et al. The effect of hydrophilic and hydrophobic structure of amphiphilic polymeric micelles on their transport in epithelial MDCK cells. *Biomaterials*. 2013;34(26):6284–6298. doi:10.1016/j.biomaterials.2013.05.006
56. Sudbery PE. Growth of *Candida albicans* hyphae. *Nat Rev Microbiol*. 2011;9(10):737–748. doi:10.1038/nrmicro2636
57. Gulati M, Nobile CJ. *Candida albicans* biofilms: development, regulation, and molecular mechanisms. *Microbes Infect*. 2016;18(5):310–321. doi:10.1016/j.micinf.2016.01.002
58. Gorka AP, Nani RR, Schnermann MJ. Harnessing cyanine reactivity for optical imaging and drug delivery. *Acc Chem Res*. 2018;51(12):3226–3235. doi:10.1021/acs.accounts.8b00384
59. Stackova L, Stacko P, Klan P. Approach to a substituted heptamethine cyanine chain by the ring opening of zincke salts. *J Am Chem Soc*. 2019;141(17):7155–7162. doi:10.1021/jacs.9b02537
60. Wang X, Zhong X, Li J, Liu Z, Cheng L. Inorganic nanomaterials with rapid clearance for biomedical applications. *Chem Soc Rev*. 2021;50(15):8669–8742. doi:10.1039/d0cs00461h
61. Shakya AK, Al-Sulaibi M, Naik RR, Nsairat H, Suboh S, Abulaila A. Review on PLGA polymer based nanoparticles with antimicrobial properties and their application in various medical conditions or infections. *Polymers*. 2023;15(17):3597. doi:10.3390/polym15173597
62. van Etten EW, Snijders SV, van Vianen W, Bakker-Woudenberg IA. Superior efficacy of liposomal amphotericin B with prolonged circulation in blood in the treatment of severe candidiasis in leukopenic mice. *Antimicrob Agents Chemother*. 1998;42(9):2431–2433. doi:10.1128/AAC.42.9.2431
63. Nami S, Aghebaty-Maleki A, Aghebaty-Maleki L. Current applications and prospects of nanoparticles for antifungal drug delivery. *EXCLI J*. 2021;20:562–584. doi:10.17179/excli2020-3068
64. Allen TM, Cullis PR. Liposomal drug delivery systems: from concept to clinical applications. *Adv Drug Deliv Rev*. 2013;65(1):36–48. doi:10.1016/j.addr.2012.09.037

International Journal of Nanomedicine

Dovepress

Publish your work in this journal

The International Journal of Nanomedicine is an international, peer-reviewed journal focusing on the application of nanotechnology in diagnostics, therapeutics, and drug delivery systems throughout the biomedical field. This journal is indexed on PubMed Central, MedLine, CAS, SciSearch®, Current Contents®/Clinical Medicine, Journal Citation Reports/Science Edition, EMBASE, Scopus and the Elsevier Bibliographic databases. The manuscript management system is completely online and includes a very quick and fair peer-review system, which is all easy to use. Visit <http://www.dovepress.com/testimonials.php> to read real quotes from published authors.

Submit your manuscript here: <https://www.dovepress.com/international-journal-of-nanomedicine-journal>